J. Non-Newtonian Fluid Mech. 159 (2009) 50–63

Contents lists available at ScienceDirect

Journal of Non-Newtonian Fluid Mechanics

journal homepage: www.elsevier.com/locate/jnnfm

Analytical solution of mixed electro-osmotic/pressure driven flows of viscoelastic fluids in microchannels

A.M. Afonso [a], M.A. Alves [a], F.T. Pinho [b,*]

[a] Departamento de Engenharia Química, Centro de Estudos de Fenómenos de Transporte, Faculdade de Engenharia da Universidade do Porto, Rua Dr. Roberto Frias s/n, 4200-465, Porto, Portugal

[b] Departamento de Engenharia Mecânica e Gestão Industrial, Centro de Estudos de Fenómenos de Transporte, Faculdade de Engenharia da Universidade do Porto, Rua Dr. Roberto Frias s/n, 4200-465, Porto, Portugal

ARTICLE INFO

Article history:
Received 2 June 2008
Received in revised form 5 December 2008
Accepted 26 January 2009

Keywords:
Electro-osmotic/pressure driven flows
PTT model
FENE-P model
Viscoelastic fluids
Microchannels
Streaming potential

ABSTRACT

Analytical solutions are presented for the flow of viscoelastic fluids in micron sized ducts, namely between parallel plates and pipes under the combined influence of electrokinetic and pressure forces using the Debye–Hückel approximation, including the limit case of pure electro-osmotic flow. The viscoelastic fluids used are described by the simplified Phan-Thien–Tanner model (sPTT), with linear kernel for the stress coefficient function, and zero second normal stress difference, and the FENE-P model, based on the kinetic theory for finitely extensible dumbbells with a Peterlin approximation for the average spring force. The solution is non-linear with a significant contribution arising from the coupling between the electric and pressure potentials. This term acts as a drag reducer and a drag increaser under favorable and adverse pressure gradients, respectively and contrasts with the Newtonian flow case, for which it does not exist, demonstrating that the superposition principle valid for Newtonian fluids no longer applies when non-linear viscoelastic fluid models are considered. The combined effects of fluid rheology, electro-osmotic and pressure gradient forcing on the fluid velocity distribution and fluid stresses are also discussed. The analysis of the streaming potential is also included.

1. Introduction

Pressure-driven fully developed pipe and channel flows of Newtonian fluids are simple flows described in most classical books on viscous fluid mechanics [1]. For non-Newtonian fluids the corresponding flow characteristics are also well known when their rheological descriptions are inelastic and rely on such simple models as the power-law or Bingham equations [2]. In contrast, the corresponding flows for complex materials described by quasi-linear and non-linear viscoelastic constitutive equations have only been the subject of research over the last 30 years, except for a few simple cases which have been known for a longer time. For the Phan-Thien–Tanner (PTT) model [3,4] there are several recent analytical solutions in the literature for non-homogeneous shear flow under fully developed conditions in pipes, channels and annuli [5–9]. For the FENE-P fluid [10], Oliveira [11] investigated analytically the solution for slit and pipe flows and some of these solutions for PTT and FENE-P fluids were extended by Cruz et al. to account for the presence of a Newtonian solvent [12] and the use of multimode models [13]. For the Giesekus fluid an earlier solution was derived by Schleiniger and Weinacht [14] and for the Johnson–Segalman constitutive equation the reader is referred to [15,16]. Issues of flow stability in these flows have also been investigated as reported and discussed in the introduction of Cruz and Pinho [13].

The overall impact of surface forces on flow characteristics increases as the flow scale decreases [17]. Therefore, capillary and electrokinetic effects, which may be negligible in macroscale flow processes, can become dominant or be used on purpose for flow control in microchannels and microfluidic devices [17]. The latter are relevant in the present context and arise when dielectric surfaces are brought in contact with polar fluids further enhanced by the application of external electric potentials. It is the case of separation and synthesis of biological or chemical components, such as the separation and manipulation of DNA molecules [18], biopolymers and large proteins.

Electro-osmosis is a basic electrokinetic phenomenon, where the flow of an electrolyte in a channel is induced by an external electric field applied between the inlet and outlet, after the interaction between the dielectric channel walls and the polar fluid has created near-wall layers of counter-ions within the fluid. These layers of liquid move under the action of the applied electric field whereas the neutral core is dragged and moves as a solid body [19]. The principle was first demonstrated by Reuss in 1809 [20], in an experimental

* Corresponding author.
E-mail addresses: aafonso@fe.up.pt (A.M. Afonso), mmalves@fe.up.pt (M.A. Alves), fpinho@fe.up.pt (F.T. Pinho).

0377-0257/$ – see front matter © 2009 Elsevier B.V. All rights reserved.
doi:10.1016/j.jnnfm.2009.01.006

Nomenclature

A_{chan}	cross section area of the channel (m^2)
$\bar{A}$, $\bar{B}$, $\bar{C}$ and $\bar{D}$	functions to compact equations
a_1, a_2, a_3 and b_1	coefficients of cubic equations
b	dumbbell extensibility (FENE-P model)
De	Deborah number
e	elementary charge (1.6022×10^{-19} C)
E_x	x-component of the electric gradient ($V\,m^{-1}$)
$E_{x,sp}$	streaming potential axial gradient ($V\,m^{-1}$)
$f(\tau_{kk})$	PTT stress coefficient function
H	microchannel half-height or pipe radius (m)
I'_c	conduction current per unit width ($A\,m^{-1}$)
I'_s	streaming current per unit width ($A\,m^{-1}$)
I'	net electrical current per unit width ($A\,m^{-1}$)
k_B	Boltzmann constant ($1.3807 \times 10^{-23}\,J\,K^{-1}$)
l	microchannel length (m)
n_o	ionic number concentration (m^{-3})
p	pressure (Pa)
$p_{,x}$	axial pressure gradient ($Pa\,m^{-1}$)
P_{sur}	wetted perimeter (m)
Q	volumetric flow rate ($m^3\,s^{-1}$)
t	time (s)
T	absolute temperature (K)
U_N	Newtonian bulk velocity ($m\,s^{-1}$)
u_{sh}	Helmholtz–Smoluchowski velocity ($m\,s^{-1}$)
w	microchannel width (m)
x	axial direction (m)
y	transverse coordinate (m)
z	valence of ions
$Z(\tau_{kk})$	FENE-P stress coefficient function

Tensors and vectors

$\mathbf{D}$	rate of deformation tensor (s^{-1})
$\mathbf{E}$	external applied electric field ($V\,m^{-1}$)
$\mathbf{I}$	unitary tensor
$\mathbf{u}$	velocity vector ($m\,s^{-1}$)
$\boldsymbol{\tau}$	polymeric extra stress tensor (Pa)

Greek symbols

χ	near-wall variable ($\equiv (1-\bar{y})\bar{\kappa}$)
δ	locus of velocity maximum (m)
δ_l	thickness of the skimming layer (m)
ε	PTT parameter
ϵ	dielectric constant of the fluid ($C\,V^{-1}\,m^{-1}$)
ϕ	electric potential (V)
γ	Euler–Mascheroni constant
$\dot{\gamma}$	shear rate (s^{-1})
Γ	ratio of pressure to electro-osmotic driving forces
η	polymer viscosity coefficient (PTT and FENE-P models) (Pa s)
κ^2	Debye–Hückel parameter (m^{-2})
λ	relaxation time (s)
μ	viscometric viscosity (Pa s)
ρ_e	electric charge density ($C\,m^{-3}$)
σ_t	total electric conductivity ($\Omega^{-1}\,m^{-1}$)
σ_{fluid}	fluid bulk conductivity ($\Omega^{-1}\,m^{-1}$)
σ_{sur}	wall surface conductivity (Ω^{-1})
τ_{xx}, τ_{yy}	normal stresses (Pa)
τ_{xy}	shear stress (Pa)
τ_{kk}	trace of the extra-stress tensor (Pa)
ξ	EDL thickness (m)
ψ	potential field (V)
ψ_0	wall zeta potential (V)
Υ_1	dimensionless number

Mathematical

∇	upper-convected derivative

Subscripts

sp	refers to streaming potential
N	refers to Newtonian
sh	refers to Helmholtz–Smoluchowski
x	refers to the axial coordinate
κ	refers to Debye–Hückel parameter

Superscript

E	related to electro-osmotic flow
P	related to pressure-driven flow
EP	related to pressure-driven and electro-osmotic combined effects
$\bar{}$	dimensionless quantity

investigation using porous clay. This was followed by the theoretical work on the electric double layer (EDL) of Helmholtz in 1879 [21], which related the electrical and flow parameters for electrokinetically driven flows. In the early 1900s von Smoluchowski [22] contributed to the understanding of electrokinetically driven flows, especially for conditions where the EDL thickness is much smaller than the channel height.

For Newtonian fluids, rigorous modeling of the electro-osmotic flow in microchannels has been the subject of several studies. Burgreen and Nakache [23] studied the effect of the surface potential on liquid transport through ultrafine slits relying on the Debye–Hückel linear approximation to the electrical potential distribution under an imposed electrical field. Rice and Whitehead [24] discussed the same problem in a circular capillary and Levine et al. [25] extended the Rice and Whitehead model [24] to a higher surface potential. Dutta and Beskok [26] obtained analytical solutions for the velocity distribution, mass flow rate, pressure gradient, wall shear stress, and vorticity in mixed electro-osmotic/pressure driven flows for two-dimensional straight channels, under conditions of small EDL thickness, with application to microfluidic devices where the wall-to-wall distance was one to three orders of magnitude larger than EDL thickness. Arulanandam and Li [27] and Wang et al. [28] presented a two-dimensional analytical model for the electro-osmotic flow in a microchannel with rectangular cross-section. A thorough review on various other aspects of electro-osmosis can be found in Karniadakis et al. [29].

The theoretical study of electro-osmotic flows of non-Newtonian fluids is recent and most works have been limited to simple inelastic fluid models, such as the power-law, due to the inherent analytical difficulties introduced by more complex constitutive equations. Examples are the recent works of Das and Chakraborty [30] and Chakraborty [31], who presented explicit analytical solutions for velocity, temperature and concentration distributions in electro-osmotic microchannel flows of a non-Newtonian bio-fluid described by the power-law model. Other purely viscous models were analytically investigated by Berli and Olivares [32], who considered the existence of a small wall layer depleted of additives (the skimming layer) and behaving as a Newtonian fluid under the combined action of pressure and electrical fields, thus restricting the non-Newtonian behaviour to the electrically neutral region outside the EDL. Investigations on other relevant phenomena in microfluidics, such as surface tension effects and its relation to non-Newtonian properties also rely on the inelastic power law viscosity model [33].

Very recently these studies were extended to viscoelastic fluids by Park and Lee [34], who derived the Helmholtz–Smoluchowski velocity for pure electro-osmotic flow of PTT fluids and provided a simple numerical procedure to calculate its value. It is clear that there are no analytical solutions for fully-developed electro-osmotic flows of quasi-linear and non-linear viscoelastic fluids, and even less so when in combination with pressure gradient, where some new non-linear coupled terms arise. This work aims to partially fulfill this gap by presenting the analytical solutions for the flows of PTT and FENE-P fluids between two parallel plates under the mixed influence of electrokinetic and pressure forces, including the limit case of pure electro-osmosis. The PTT fluid [3] obeys the simplified model, with a linear kernel for the stress coefficient function [4] and a zero second normal stress difference, thus it includes the solution for Upper-Convected model (UCM) fluids. The FENE-P fluid is also used, and this model is based on the kinetic theory for finitely extensible non-linear elastic dumbbells with a Peterlin approximation for the average spring force (cf. Bird et al. [10]). The viscoelastic fluids are assumed to have the same properties in the whole domain including the EDL. Bio-fluids are usually complex in their structure leading to equally complex constitutive equations to describe their rheology and the ensuing flows. In particular they often exhibit normal stresses, shear-thinning viscosity and memory effects and their rheological behaviour can be described by differential viscoelastic constitutive equations that are related to the PTT and FENE-P form, as in the case of blood [35,36], saliva [37], synovial fluid [38,39] or other biofluids containing long chain molecules. The flows of relevance here would be in micron-size geometries as in chips for chemical and biological analysis and in micro-rheometers [40].

The paper starts with the set of governing equations including the non-linear Poisson–Boltzmann equation governing the EDL field and the added body force to the momentum equation caused by the applied electrical potential field. The simplifications required to obtain the analytical solution are discussed, the solutions are presented, including the particular case of streaming potential, and a discussion of the effects of the various relevant nondimensional parameters upon the flow characteristics closes this work.

2. Governing equations

The steady, fully-developed flow of the incompressible viscoelastic fluid under investigation is sketched in Fig. 1. The flow direction in the conditions illustrated is from left to right, but it can be reversed if either the polarity at the walls or of the electrodes at each end of the channel are reversed. In both cases, the solutions here described remain valid. The migration of ions naturally arises due to the interaction between the dielectric walls and the polar fluid. Here, the two negatively charged walls of the microchannel of height $2H$, length l and width w, with $w \gg 2H$, attract counter-ions forming layers of positively charged fluid near the walls and repel the co-ions. Very thin layers of immobile counter-ions cover the walls, known as the Stern layers, followed by thicker more diffuse layers of mobile counter-ions, the two layers near the wall forming

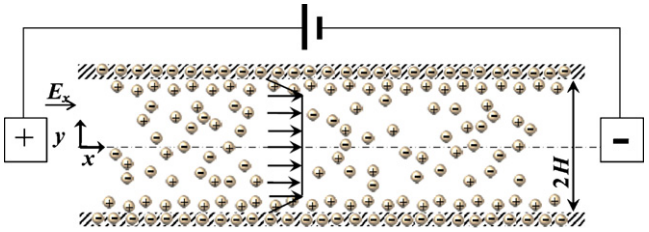

Fig. 1. Schematic of the flow in a microchannel.

what is called the electric double layer (EDL). The global charge of the flow domain remains neutral, but since the two EDLs are thin the core is essentially neutral. Applying a DC potential difference between the two electrodes at the inlet and outlet generates an external electric field that exerts a body force on the counter-ions of the EDL, which move along the channel dragging the neutral liquid core. The pressure difference that can also be applied between the inlet and outlet can act in the same direction of the electric field or in the opposite direction. Alternatively, the potential difference is not imposed, but results from the accumulation of ions at the end of the channel due to the flow created by the pressure difference. This particular case, known as streaming potential, implies a specific relation between the favorable pressure gradient and the ensuing adverse external electric field [41], which will be quantified later in this paper.

The basic field equations describing this fully-developed flow for incompressible fluids are the continuity equation,

$$\nabla \cdot \mathbf{u} = 0 \tag{1}$$

and the modified Cauchy equation,

$$-\nabla p + \nabla \cdot \boldsymbol{\tau} + \rho_e \mathbf{E} = \mathbf{0} \tag{2}$$

where $\mathbf{u}$ is the velocity vector, p the pressure, and $\boldsymbol{\tau}$ the polymeric extra-stress contribution. The $\rho_e\mathbf{E}$ term of Eq. (2) represents a body force per unit volume, where $\mathbf{E}$ is the applied external electric field (or resulting from the streaming potential) and ρ_e is the net electric charge density in the fluid.

2.1. Constitutive equations

2.1.1. PTT model

The polymer extra-stress $\boldsymbol{\tau}$ is described by an appropriate constitutive equation, and in this work we consider two models. The first model describes the viscoelastic behaviour following the ideas of Phan-Thien and Tanner [3,4], who derived the PTT model – Eq. (3)– from network theory arguments:

$$f(\tau_{kk})\boldsymbol{\tau} + \lambda \boldsymbol{\tau}^{\nabla} = 2\eta \mathbf{D} \tag{3}$$

where $\mathbf{D} = (\nabla \mathbf{u}^T + \nabla \mathbf{u})/2$ is the rate of deformation tensor, λ is the relaxation time of the fluid, η is a polymer viscosity coefficient and $\boldsymbol{\tau}^{\nabla}$ represents the upper-convected derivative of $\boldsymbol{\tau}$, defined as

$$\boldsymbol{\tau}^{\nabla} = \frac{\mathrm{D}\boldsymbol{\tau}}{\mathrm{D}t} - \nabla \mathbf{u}^T . \boldsymbol{\tau} - \boldsymbol{\tau} . \nabla \mathbf{u} \tag{4}$$

The stress coefficient function, $f(\tau_{kk})$, is given by the linear form [3]

$$f(\tau_{kk}) = 1 + \frac{\varepsilon \lambda}{\eta} \tau_{kk} \tag{5}$$

where τ_{kk} represents the trace of the extra-stress tensor and ε is a parameter that imposes an upper limit to the elongational viscosity. For $\varepsilon = 0$ the upper-convected Maxwell model (UCM) is recovered.

2.1.2. FENE-P model

The second viscoelastic model used in this work is the FENE-P equation, based on the kinetic theory for finitely extensible dumbbells with a Peterlin approximation for the average spring force. In this case the polymer extra-stress is given by [10]:

$$Z(\tau_{kk})\boldsymbol{\tau} + \lambda \boldsymbol{\tau}^{\nabla} - \lambda \left(\boldsymbol{\tau} - \frac{b}{b+2} n k_B T \mathbf{I} \right) \frac{\mathrm{D} \ln Z}{\mathrm{D}t} = 2\eta \left(\frac{b+5}{b+2} \right) \mathbf{D} \tag{6}$$

where $\mathbf{I}$ is the identity tensor, b is a parameter that measures the extensibility of the dumbbell, k_B is the Boltzmann constant, T is the absolute temperature and n is a parameter of the model [10]. The stress coefficient function, $Z(\tau_{kk})$, can be expressed by [10]:

$$Z(\tau_{kk}) = 1 + 3 \left(\frac{1}{b+2} + \frac{\lambda}{3\eta} \frac{\tau_{kk}}{(b+5)} \right) \tag{7}$$

Note that for fully-developed flows $D \ln Z/Dt \approx 0$ and Eq. (6) becomes considerably simplified.

2.2. Poisson–Boltzmann equation

Contact between the dielectric walls of the channel with the electrolyte fluid spontaneously results in the formation of two electric double layers, one near each wall, as seen in Fig. 1. They are sufficiently far from each other to allow us to consider them as independent. In the case of pipe flow there is a single EDL around the wall, so that EDL's at opposite sides of a diameter do not interfere. The potential field (ψ) of these electric double layers can be expressed by means of a Poisson–Boltzmann equation:

$$\nabla^2\psi = -\frac{\rho_e}{\epsilon} \tag{8}$$

where ϵ is the dielectric constant of the solution, assumed constant. The Poisson–Boltzman equation can be integrated subjected to adequate boundary conditions, to be given in the next section. Prior to that it is necessary to quantify the electric charge density in order to have a closed-form equation. According to Bruus [19] the electric charge density, ρ_e, for an electrolyte in equilibrium near a charged surface is given by

$$\rho_e = -2n_o ez \sinh\left(\frac{ez}{k_B T}\psi\right) \tag{9}$$

where n_o is the ionic density, e is the elementary electronic charge and z is the valence of the ions.

2.3. Boundary conditions and other assumptions

The coordinate system is represented in Fig. 1. Due to the symmetry of the geometry only half of the channel ($0 \le y \le H$) is considered in this analysis. For the pipe geometry, H is the pipe radius. At the wall the no-slip condition applies whereas on the centreplane/axis, $y = 0$, the condition of symmetry applies. Since the flow is fully-developed the velocity and stress fields only depend on the transverse coordinate y. This coordinate represents the radial position for the pipe flow.

As described above, the contact between the dielectric wall and the electrolyte fluid results in a spontaneous charge transfer between wall and fluid by ionization, ion adsorption or ion dissolution that leads to an opposite charge distribution at the wall and fluid, which depends on the chemical composition of both materials, while maintaining global charge neutrality. Then, electro-osmotic flow results from the motion of the charged fluid species when subjected to an externally applied electric field between the channel/pipe inlet and outlet. The thickness of the EDL depends on the ionic concentration, thermal energy and electrical properties of the liquid, ranging from nanometers for high ionic concentration solutions to several microns for pure water and pure organic liquids. Here, we assume that the ionic charge distribution across the channel/pipe is such that the two EDL are thin. Under these conditions and provided the applied electric field is weak, i.e., that $\triangle\phi/l \ll \psi_0/\xi$, where $\triangle\phi$ is the potential difference of the applied electric field, l is the channel length and ξ is the Debye layer thickness, the charge distribution is essentially independent of the external electric field and is determined from the potential at the wall, ψ_0, frequently called the zeta potential. If the local electro-osmotic flow velocities are small, which is the case for thin EDL, the effect of fluid motion on the charge redistribution can also be neglected. These assumptions are all part of the so-called standard electrokinetic model.

The electric double layer is thin when the potential at the wall is small. For small values of $ez\psi_0/k_BT$, synonymous of a small ratio of electrical to thermal energies, Eq. (9) can be linearized, $\sinh x \approx x$. This is called the Debye–Hückel approximation and is invoked in this work. At room temperature this limits the zeta potential to values much smaller than 26 mV. Under these conditions, each wall only affects the charge distribution in its vicinity and does not interfere with the charge distribution near the other wall of the channel. For thin layers in a pipe this also means that there is no need to account for wall curvature effects, when deriving the potential and electric charge distributions for the pipe flow solution.

The boundary conditions for the Poisson–Boltzmann equation are $\partial\psi/\partial y = 0$ at the symmetry plane/axis and zeta potential at the wall, $\psi_{\text{wall}} = \psi_0$, which takes the sign of the fluid charges at the wall.

Regarding the non-Newtonian fluid, the assumption is made that there is a well mixed fluid behaviour uniformly distributed across the channel/pipes. An alternative assumption, sometimes invoked for solutions and suspensions, including non-Newtonian fluids [32], is that there is depletion of additives very close to the wall, where the fluid essentially behaves as a Newtonian fluid. This is currently under investigation and the corresponding solution is considerably more elaborate. Besides there are here possibilities that need to be considered, and this matter is left for future work.

3. Analytical solution

3.1. PTT constitutive equation

The extra-stresses for the PTT model in these fully-developed flows, for which $\mathbf{u} = \{u(y), 0, 0\}$, can be obtained from Eqs. (3)–(5), which reduce to

$$f(\tau_{kk})\tau_{xx} = 2\lambda\dot{\gamma}\tau_{xy} \tag{10}$$

$$f(\tau_{kk})\tau_{yy} = 0 \tag{11}$$

$$f(\tau_{kk})\tau_{xy} = \eta\dot{\gamma} + \lambda\dot{\gamma}\tau_{yy} \tag{12}$$

where $\tau_{kk} = \tau_{xx} + \tau_{yy}$ is the trace of the extra-stress tensor. Eq. (11) implies $\tau_{yy} = 0$, $\tau_{kk} = \tau_{xx}$, and the stress coefficient function becomes an explicit function of the streamwise normal stress $f(\tau_{xx})$ as in [3]. Then, upon division of Eq. (10) by Eq. (12) the specific function $f(\tau_{xx})$ cancels out, and a relation between the normal and shear stresses is obtained,

$$\tau_{xx} = 2\frac{\lambda}{\eta}\tau_{xy}^2 \tag{13}$$

3.2. FENE-P constitutive equation

For the FENE-P fluid in fully developed shear flow between two parallel plates and in a pipe, i.e., subjected to $\mathbf{u} = \{u(y), 0, 0\}$, Eqs. (6) and (7) reduce to

$$Z(\tau_{kk})\tau_{xx} = 2\lambda\dot{\gamma}\tau_{xy} \tag{14}$$

$$Z(\tau_{kk})\tau_{xy} = \left(\frac{b+5}{b+2}\right)\eta\dot{\gamma} \tag{15}$$

Again, the trace of the extra-stress tensor becomes $\tau_{kk} = \tau_{xx}$, thus

$$Z(\tau_{xx}) = \left(\frac{b+5}{b+2}\right)\left[1 + \frac{\lambda}{\eta}\frac{(b+2)}{(b+5)^2}\tau_{xx}\right] \tag{16}$$

The relation between the normal and shear stresses is,

$$\tau_{xx} = 2\frac{\lambda}{\eta}\left(\frac{b+2}{b+5}\right)\tau_{xy}^2 \tag{17}$$

3.3. Potential field across the channel

The potential field only depends on y, $\nabla^2\psi = \mathrm{d}^2\psi/\mathrm{d}y^2$, which can be used in Eq. (8). Substituting the distribution of the net charge

density (ρ_e) by Eq. (9) and invoking the assumptions discussed in Section 2.3, the following form of the Poisson–Boltzmann equation for the potential across the half channel is obtained:

$$\frac{d^2\psi}{dy^2} = \kappa^2\psi \tag{18}$$

where $\kappa^2 = ((2n_o e^2 z^2)/(\epsilon k_B T))$ is the Debye–Hückel parameter, related to the thickness of the Debye layer, $\xi = 1/\kappa$ (also referred to as the EDL thickness). This approximation is valid when the Debye thickness is small but finite, i.e., for $10 \lesssim H/\xi \lesssim 10^3$, and it is also used here for pipe flow neglecting wall curvature effects in the Laplacian.

Eq. (18) can be solved subjected to the boundary conditions (cf. Section 2.3) to give,

$$\psi = \frac{\psi_0 \cosh(\kappa y)}{\cosh(\kappa H)} \tag{19}$$

for $0 \le y \le H$. Finally, the net charge density distribution, Eq. (9), in conjunction with Eq. (19) reduces to

$$\rho_e = -\epsilon\psi_0\kappa^2 \frac{\cosh(\kappa y)}{\cosh(\kappa H)} \tag{20}$$

which is a positive quantity for a wall charged negatively ($\psi_0 < 0$).

3.4. Analytical solution for the PTT model

Henceforth, the analytical solution and the subsequent discussions are for channel flow, thus avoiding unnecessary complications. The full solution for pipe flow is presented in Appendix A without any discussion because the trends are similar to those found for the slit flow.

Under fully developed conditions, the momentum Eq. (2), reduces to

$$\frac{d\tau_{xy}}{dy} = -\rho_e E_x + p_{,x} \tag{21}$$

where $p_{,x} \equiv dp/dx$, $E_x \equiv -d\phi/dx$ and ϕ is the electric potential of the applied external field, which is characterized by a constant streamwise gradient under fully-developed flow conditions. Note that in this flow the external electrical field is positive according to Fig. 1, and negative otherwise.

Using Eq. (20) and noting that the shear stress at the centerline is zero, Eq. (21) can be integrated to yield the following linear contribution of electro-osmotic and pressure gradient contributions to the shear stress distribution

$$\tau_{xy} = \epsilon\psi_0 E_x \kappa \frac{\sinh(\kappa y)}{\cosh(\kappa H)} + p_{,x} y \tag{22}$$

Using the relation between the normal and shear stresses—Eq. (13), the following explicit expression for the normal stress component is obtained,

$$\tau_{xx} = 2\frac{\lambda}{\eta}\left(\epsilon\psi_0 E_x \kappa \frac{\sinh(\kappa y)}{\cosh(\kappa H)} + p_{,x} y\right)^2 \tag{23}$$

The square term in Eq. (23) introduces a contribution to the normal stress from the combined electro-osmotic and pressure forces.

To determine the velocity gradient, Eqs. (12), (22) and (23) are combined to give

$$\dot\gamma \equiv \frac{du}{dy} = \left[1 + 2\varepsilon\lambda^2\left(\frac{\kappa\epsilon\psi_0 E_x}{\eta}\frac{\sinh(\kappa y)}{\cosh(\kappa H)} + \frac{p_{,x}}{\eta} y\right)^2\right] \times \left(\frac{\kappa\epsilon\psi_0 E_x}{\eta}\frac{\sinh(\kappa y)}{\cosh(\kappa H)} + \frac{p_{,x}}{\eta} y\right) \tag{24}$$

Eq. (24) can be integrated subject to the no-slip boundary condition at the wall ($u_{\|y=H} = 0$) and the resulting velocity profile is

$$u = u^E + u^P + u^{EP} \tag{25}$$

with

$$u^E = \left(\frac{\epsilon\psi_0 E_x}{\eta} - 2\bar C\kappa^2\varepsilon\lambda^2\left[\frac{\epsilon\psi_0 E_x}{\eta}\right]^3\right)(\bar A - 1) + \frac{2}{3}\kappa^2\varepsilon\lambda^2\left[\frac{\epsilon\psi_0 E_x}{\eta}\right]^3 \times (\bar A^3 - 1) \tag{26}$$

$$u^P = \frac{1}{2}\left[\frac{p_{,x}}{\eta}\right](y^2 - H^2)\left[1 + \varepsilon\lambda^2\left[\frac{p_{,x}}{\eta}\right]^2(y^2 + H^2)\right] \tag{27}$$

$$u^{EP} = \frac{3}{2}\varepsilon\lambda^2\left[\frac{\epsilon\psi_0 E_x}{\eta}\right]^2\left[\frac{p_{,x}}{\eta}\right][1 - \bar A^2 + (\kappa^2H^2 - \kappa^2y^2)\bar C + 2\kappa\bar D(y\bar A\bar B - H)] + 12\frac{\varepsilon\lambda^2}{\kappa^2}\left[\frac{\epsilon\psi_0 E_x}{\eta}\right]\left[\frac{p_{,x}}{\eta}\right]^2\left[\kappa\bar D(H - y\bar B) + \left(1 + \frac{1}{2}\kappa^2y^2\right)\bar A - \left(1 + \frac{1}{2}\kappa^2H^2\right)\right] \tag{28}$$

where $\bar A = ((\cosh(\kappa y))/(\cosh(\kappa H)))$, $\bar B = ((\sinh(\kappa y))/(\sinh(\kappa H)))$, $\bar C = (1/(\cosh^2(\kappa H)))$ and $\bar D = \tanh(\kappa H)$.

As suggested by Eq. (25) there are three contributions to the velocity profile: u^E represents the pure electro-osmotic flow for a viscoelastic fluid and is given by Eq. (26); u^P is the contribution due to the pressure gradient for a viscoelastic fluid and is given by Eq. (27); finally, the third contribution couples the Poiseuille and electro-osmotic flows and this is given by u^{EP} expressed by Eq. (28), which is simultaneously proportional to $p_{,x}$ and E_x. This last contribution only exists because the fluid is non-linear, i.e., no such effect is present if the fluid is Newtonian or a quasi-linear viscoelastic fluid, such as UCM fluid. Indeed, u^{EP} is proportional to ε, which is non-zero for the PTT fluid but is zero for UCM/Oldroyd-B fluids. Eq. (25) shows that the superposition principle valid for Newtonian and quasi-linear viscoelastic fluids is no longer valid for the PTT and FENE-P fluids and suggests that the same applies to other non-linear viscoelastic models.

It is often more convenient to work with the dimensionless form of Eq. (25). Introducing the normalizations $\bar y = y/H$ and $\bar\kappa = \kappa H$, the dimensionless velocity profile can be written as

$$\frac{u}{u_{sh}} = (1 - 2\bar C\varepsilon De_\kappa^2)(1 - \bar A) + \frac{2}{3}\varepsilon De_\kappa^2(1 - \bar A^3) - \frac{1}{2}\Gamma(1 - \bar y^2) \times \left[1 + \frac{\varepsilon De_\kappa^2}{\bar\kappa^2}\Gamma^2(1 + \bar y^2)\right] + \frac{3}{2}\frac{\varepsilon De_\kappa^2}{\bar\kappa^2}\Gamma[1 - \bar A^2 + (\bar\kappa^2 - (\bar\kappa\bar y)^2)\bar C + 2\bar\kappa\bar D(\bar y\bar A\bar B - 1)] - \frac{12\varepsilon De_\kappa^2}{\bar\kappa^4}\Gamma^2\left[\bar\kappa\bar D(1 - \bar y\bar B) + \left(1 + \frac{1}{2}(\bar\kappa\bar y)^2\right)\bar A - \left(1 + \frac{1}{2}\bar\kappa^2\right)\right] \tag{29}$$

where $De_\kappa = ((\lambda u_{sh})/\xi) = \lambda\kappa u_{sh}$ is the Deborah number based on the EDL thickness and on the Helmholtz–Smoluchowski electro-osmotic velocity, defined as $u_{sh} = -((\epsilon\psi_0 E_x)/\eta)$ [22,34]. In Poiseuille flows a different Deborah number is usually defined [5,7] based on the cross-sectional average velocity for the Newtonian flow under the sole influence of pressure gradient and the channel half-height, $De_N = ((\lambda U_N)/H)$ with $U_N = -((H^2 p_{,x})/3\eta)$. A third alternative Deborah number for electro-osmotic flow is based again on u_{sh}, but considers the channel half-height, $De_{sh} = ((\lambda u_{sh})/H)$. These three Deborah numbers are related by $De_\kappa = \bar\kappa De_{sh} = -(3/\Gamma)\bar\kappa De_N$, where parameter $\Gamma = -(H^2/(\epsilon\psi_0))(p_{,x}/E_x)$ represents the ratio of pressure to electro-osmotic driving forces.

Flow problems are usually of direct or indirect/inverse type. In a direct problem the pressure gradient $p_{,x}$ and the applied electric potential gradient E_x are known (or instead the ratio of pressure to electro-osmotic driving forces is known) and the flow rate, or the cross-sectional average velocity, is required. The flow rate can be determined from integration of the velocity profile of Eq. (25). Here, this integration was carried out using the normalized velocity profile, Eq. (29), thinking ahead on the benefit this brings to the inverse problem, where the aim is the determination of Γ for a given dimensionless flow rate. The expression for the normalized flow rate is

$$\begin{aligned}
&\bar{Q} = \frac{Q}{2Hu_{sh}} = \frac{\bar{u}}{u_{sh}} = \int_{-1}^{1} \frac{u}{u_{sh}} \mathrm{d}\bar{y} = 2\int_{0}^{1} \frac{u}{u_{sh}} \mathrm{d}\bar{y} = \bar{Q}^{E} + \bar{Q}^{P} + \bar{Q}^{EP} \\
&\bar{Q}^{E} = 2(1 - 2\bar{C}\varepsilon De_{\kappa}^{2})\left(1 - \frac{\bar{D}}{\bar{\kappa}}\right) + \frac{4}{3}\varepsilon De_{\kappa}^{2}\left(1 - \frac{1}{3}\frac{\bar{D}}{\bar{\kappa}}(1 + 2\bar{C})\right) \\
&\bar{Q}^{P} = -2\Gamma\left(\frac{2}{5}\frac{\varepsilon De_{\kappa}^{2}}{\bar{\kappa}^{2}}\Gamma^{2} + \frac{1}{3}\right) \\
&\bar{Q}^{EP} = 3\frac{\varepsilon De_{\kappa}^{2}}{\bar{\kappa}^{2}}\Gamma\left(2 - \frac{\bar{D}}{\bar{\kappa}} - \bar{C} + \frac{2}{3}\bar{C}\bar{\kappa}^{2} - 2\bar{\kappa}\bar{D}\right) - \frac{24\varepsilon De_{\kappa}^{2}}{\bar{\kappa}^{4}}\Gamma^{2}\left(-3 + 3\frac{\bar{D}}{\bar{\kappa}} + \frac{3}{2}\bar{\kappa}\bar{D} - \frac{1}{2}\bar{\kappa}^{2}\right)
\end{aligned} \tag{30}$$

This is a cubic equation on Γ and the solution of the inverse problem (calculation of Γ for a given $\bar{Q}$) involves the determination of Γ, which can be done using the Cardan–Tartaglia solution for cubic algebraic equations. Within the assumptions invoked in Section 2.3, the analysis in this section is general, but relies on the Debye–Hückel approximation. Here, as in many practical applications the finite electric double layer is very small, about 1–3 orders of magnitude smaller than the thickness of the microfluidic channel ($10 \lesssim \bar{\kappa} \lesssim 10^{3}$). In these circumstances $\cosh(\bar{\kappa}) \gg 1$ and $\bar{D} = \tanh(\bar{\kappa}) \approx 1$, so the above equations for the velocity profile can be further simplified. In particular the normalized flow rate becomes

$$\begin{aligned}
\bar{Q} \simeq\ & 2\left(\frac{\bar{\kappa} - 1}{\bar{\kappa}}\right) + \frac{4}{3}\varepsilon De_{\kappa}^{2}\left(\frac{3\bar{\kappa} - 1}{3\bar{\kappa}}\right) - 2\Gamma\left(\frac{2}{5}\frac{\varepsilon De_{\kappa}^{2}}{\bar{\kappa}^{2}}\Gamma^{2} + \frac{1}{3}\right) \\
&+ 3\frac{\varepsilon De_{\kappa}^{2}}{\bar{\kappa}^{2}}\Gamma\left(\frac{2\bar{\kappa} - 1 - 2\bar{\kappa}^{2}}{\bar{\kappa}}\right) - \frac{24\varepsilon De_{\kappa}^{2}}{\bar{\kappa}^{4}}\Gamma^{2}\left(\frac{\bar{\kappa}}{2}(3 - \bar{\kappa}) + \frac{3 - 3\bar{\kappa}}{\bar{\kappa}}\right)
\end{aligned} \tag{31}$$

which is simpler than Eq. (30), but still cubic in Γ. This expression can be written in compact form as

$$\Gamma^{3} + a_{1}\Gamma^{2} + a_{2}\Gamma + a_{3} = 0 \tag{32}$$

The explicit solution of the inverse problem, giving the ratio of pressure to electro-osmotic driving forces as a function of the non-dimensional flow rate, viscoelastic model parameters and relative microchannel ratio is obtained using the Cardan–Tartaglia solution,

$$\begin{aligned}
&\Gamma = \sqrt[3]{-\frac{b_{1}}{2} + \sqrt{\frac{b_{1}^{2}}{4} + \frac{a^{3}}{27}}} + \sqrt[3]{-\frac{b_{1}}{2} - \sqrt{\frac{b_{1}^{2}}{4} + \frac{a^{3}}{27}}} - \frac{a_{1}}{3} \\
&a = a_{2} - \frac{a_{1}^{2}}{3} \\
&b_{1} = a_{3} - \frac{a_{1}a_{2}}{3} + \frac{2a_{1}^{3}}{27}
\end{aligned} \tag{33}$$

with

$$\begin{aligned}
&a_{1} = 15\left(\frac{3 - \bar{\kappa}}{\bar{\kappa}}\right) + 30\left(\frac{3 - 3\bar{\kappa}}{\bar{\kappa}^{3}}\right) \\
&a_{2} = \frac{5}{6}\frac{\bar{\kappa}^{2}}{\varepsilon De_{\kappa}^{2}} + \frac{15}{4}\left(\frac{2\bar{\kappa}^{2} - 2\bar{\kappa} + 1}{\bar{\kappa}}\right) \\
&a_{3} = \frac{5}{4}\frac{\bar{\kappa}^{2}}{\varepsilon De_{\kappa}^{2}}\left(\bar{Q} - 2\left(\frac{\bar{\kappa} - 1}{\bar{\kappa}}\right) - \frac{4}{3}\varepsilon De_{\kappa}^{2}\left(\frac{3\bar{\kappa} - 1}{3\bar{\kappa}}\right)\right)
\end{aligned} \tag{34}$$

The explicit expressions for the dimensionless shear and normal stress components are obtained from normalization of Eqs. (22) and (23),

$$\frac{\tau_{xy}}{3\eta u_{sh}\kappa} = \frac{1}{3}\left[\Gamma\frac{\bar{y}}{\bar{\kappa}} - \frac{\sinh(\bar{\kappa}\bar{y})}{\cosh(\bar{\kappa})}\right] \tag{35}$$

$$\frac{\tau_{xx}}{3\eta u_{sh}\kappa} = \frac{2}{3}De_{\kappa}\left(\Gamma\frac{\bar{y}}{\bar{\kappa}} - \frac{\sinh(\bar{\kappa}\bar{y})}{\cosh(\bar{\kappa})}\right)^{2} \tag{36}$$

The normalized shear rate is

$$\frac{\dot{\gamma}}{u_{sh}\kappa} = \left[1 + 2\varepsilon De_{\kappa}^{2}\left(\Gamma\frac{\bar{y}}{\bar{\kappa}} - \frac{\sinh(\bar{\kappa}\bar{y})}{\cosh(\bar{\kappa})}\right)^{2}\right]\left(\Gamma\frac{\bar{y}}{\bar{\kappa}} - \frac{\sinh(\bar{\kappa}\bar{y})}{\cosh(\bar{\kappa})}\right) \tag{37}$$

and the viscosity profile is given by

$$\mu(\dot{\gamma}) \equiv \frac{\tau_{xy}}{\dot{\gamma}} \Rightarrow \frac{\mu(\dot{\gamma})}{\eta} = \left[1 + 2\varepsilon De_{\kappa}^{2}\left(\Gamma\frac{\bar{y}}{\bar{\kappa}} - \frac{\sinh(\bar{\kappa}\bar{y})}{\cosh(\bar{\kappa})}\right)^{2}\right]^{-1} \tag{38}$$

Wall values for all these quantities are useful and are obtained after setting $\bar{y} = 1$ (and $\tanh(\bar{\kappa}) \approx 1$ for $\bar{\kappa} \gtrsim 10$):

$$\begin{aligned}
&\left.\frac{\tau_{xy}}{3\eta u_{sh}\kappa}\right|_{w} \simeq \frac{1}{3}\left(\frac{\Gamma}{\bar{\kappa}} - 1\right) \\
&\left.\frac{\tau_{xx}}{3\eta u_{sh}\kappa}\right|_{w} \simeq \frac{2}{3}De_{\kappa}\left(\frac{\Gamma}{\bar{\kappa}} - 1\right)^{2} \\
&\left.\frac{\mu(\dot{\gamma})}{\eta}\right|_{w} \simeq \left[1 + 2\varepsilon De_{\kappa}^{2}\left(\frac{\Gamma}{\bar{\kappa}} - 1\right)^{2}\right]^{-1}
\end{aligned} \tag{39}$$

The dimensionless locci of the local velocity profile maximum (or minimum), $\bar{\delta}$, can be obtained by setting the shear rate Eq. (37) to zero. Since the first term on the right-hand side of Eq. (37) is always positive, $\bar{\delta}$ requires the multiplicative factor to be null and is given by,

$$\bar{\delta} = \frac{\bar{\kappa}}{\Gamma}\frac{\sinh(\bar{\kappa}\bar{\delta})}{\cosh(\bar{\kappa})} = \frac{\bar{\kappa}}{\Gamma}\overline{B(\bar{\delta})} \tag{40}$$

This is an interesting equation, because it is independent of the fluid rheology. Recalling Eq. (35) it implies that $\tau_{xy\|\bar{y}=\bar{\delta}} = 0$, and obviously $\bar{\delta} = 0$ is a natural solution of Eq. (40) required by the centerline symmetry condition. However Eq. (40) must have a second solution for $\bar{\delta}$ for positive values of Γ as will become apparent in Section 4(cf. Fig. 3).

3.5. Streaming potential solution

In the solution of the previous section, the electrical field E_x can be applied externally or be a consequence of electric potentials created by the flow. In the absence of an externally applied electrical field, the imposed pressure difference causes a flow containing ions in motion, hence it causes an electrical current, called the streaming current, I_s'. The streaming current accumulates counterions at the end of the channel therefore setting up an electric field, $E_{x,sp}$ which is associated with the so-called streaming potential, ϕ_{sp} via $E_{x,sp} = -\Delta\phi_{sp}/l$. Therefore, this induced electric field opposes the flow and creates an opposite current, I_c', called conduction corrent.

The net electrical current, I', is the sum of the streaming current and the electrical conduction corrent and in steady-state should be zero:

$$I' = I'_s + I'_c \equiv 0 \tag{41}$$

The electrical streaming current (per unit of width) is of the form:

$$I'_s = 2\int_0^H u(y)\rho_e(y)\,dy \tag{42}$$

which for the particular case of the PTT fluid leads to

$$\begin{aligned}\frac{I'_s}{\epsilon\psi_0} &= \kappa\left[\frac{\epsilon\psi_0 E_{x,sp}}{\eta}\right]\left[\bar{D} - \kappa H\bar{C} + \kappa^2\varepsilon\lambda^2\left[\frac{\epsilon\psi_0 E_{x,sp}}{\eta}\right]^2\right.\\ &\times\left.\left[\bar{D} + \frac{3}{2}\kappa H\bar{C}^2 - \frac{5}{2}\bar{D}\bar{C}\right]\right] + \frac{2}{\kappa}\left[\frac{p_{,x}}{\eta}\right]\\ &\times\left[\kappa H - \bar{D} + \frac{[(p_{,x}/\eta)]^2 2\varepsilon\lambda^2}{\kappa^2}(\kappa^3H^3 - 6\bar{D} - 3\kappa^2H^2\bar{D} + 6\kappa H)\right]\\ &+ 4\kappa\varepsilon\lambda^2\left[\frac{\epsilon\psi_0 E_{x,sp}}{\eta}\right]^2\left[\frac{p_{,x}}{\eta}\right]\left[-\frac{1}{3}\bar{D} + \kappa H\bar{D}^2 - 2\kappa H\bar{C} + \frac{7}{3}\bar{D}\bar{C}\right]\\ &+ 2\frac{\varepsilon\lambda^2}{\kappa}\left[\frac{\epsilon\psi_0 E_{x,sp}}{\eta}\right]\left[\frac{p_{,x}}{\eta}\right]^2\left[3\kappa^2H^2\bar{D} - 12\kappa H\bar{D}^2 + \frac{3}{2}\bar{D}\right.\\ &\left.- \kappa^3H^3\bar{C} + 9\kappa H - \frac{21}{2}\kappa H\bar{C}\right]\end{aligned} \tag{43}$$

The electrical conduction current in the channel can now be expressed as

$$I'_c = 2\sigma_t E_{x,sp} H \tag{44}$$

where σ_t is the total electric conductivity. Note that the conduction current can now flow back through both the fluid as well as the channel walls, depending on the corresponding electrical conductivities. The total electrical conductivity can be calculated as $\sigma_t = \sigma_{\text{fluid}} + \sigma_{\text{sur}}P_{\text{sur}}/A_{\text{chan}}$, where P_{sur} and A_{chan} are the wetting perimeter and cross-section area of the channel, respectively and σ_{fluid} and σ_{sur} are the fluid bulk and wall surface conductivities, respectively. This equation and the condition imposed by Eq. (41) leads finally to the expression that defines the relation for the ratio between the imposed pressure gradient and the ensuing streaming electric field, $E_{x,sp}$. This ratio is $\Gamma_{sp} = -(H^2/(\epsilon\psi_0))(p_{,x}/E_{x,sp})$ and such relation is Eq. (45)

$$\begin{aligned}-2\Upsilon_1 &= \bar{\kappa}\bar{D} - \bar{\kappa}^2\bar{C} + 9\frac{\bar{\kappa}^3\varepsilon De_N^2}{\Gamma_{sp}^2}\left(\bar{D} + \frac{3}{2}\bar{\kappa}\bar{C}^2 - \frac{5}{2}\bar{D}\bar{C}\right)\\ &- \frac{2}{\bar{\kappa}}\Gamma_{sp}\left[\bar{\kappa} - \bar{D} + \frac{18\varepsilon De_N^2}{\bar{\kappa}^2}\left(\bar{\kappa}^3 - 6\bar{D} - 3\bar{\kappa}^2\bar{D} + 6\bar{\kappa}\right)\right]\\ &- 36\frac{\bar{\kappa}\varepsilon De_N^2}{\Gamma_{sp}}\left[-\frac{1}{3}\bar{D} + \bar{\kappa}\bar{D}^2 - 2\bar{\kappa}\bar{C} + \frac{7}{3}\bar{D}\bar{C}\right]\\ &+ 18\frac{\varepsilon De_N^2}{\bar{\kappa}}\left[3\bar{\kappa}^2\bar{D} - 12\bar{\kappa}\bar{D}^2 + \frac{3}{2}\bar{D} - \bar{\kappa}^3\bar{C} + 9\bar{\kappa} - \frac{21}{2}\bar{\kappa}\bar{C}\right]\end{aligned} \tag{45}$$

with $\Upsilon_1 = ((H^2\eta\sigma_t)/(\epsilon^2\psi_0^2))$. This new dimensionless number quantifies the effect of electric conductivity. Eq. (45) is a cubic equation in Γ_{sp}, that can be rewritten in compact form as

$$\Gamma_{sp}^3 + a_1\Gamma_{sp}^2 + a_2\Gamma_{sp} + a_3 = 0 \tag{46}$$

with coefficients

$$\begin{aligned}a_1 &= \frac{-(\bar{\kappa}\Upsilon_1 + 0.5\bar{\kappa}^2\bar{D} - 0.5\bar{\kappa}^3\bar{C} + 9\varepsilon De_N^2[3\bar{\kappa}^2\bar{D} - 12\bar{\kappa}\bar{D}^2 + (3/2)\bar{D} - \bar{\kappa}^3\bar{C} + 9\bar{\kappa} - (21/2)\bar{\kappa}\bar{C}])}{\bar{\kappa} - \bar{D} + ((18\varepsilon De_N^2)/\bar{\kappa}^2)\left(\bar{\kappa}^3 - 6\bar{D} - 3\bar{\kappa}^2\bar{D} + 6\bar{\kappa}\right)}\\ a_2 &= \frac{18\bar{\kappa}^2\varepsilon De_N^2[-(1/3)\bar{D} + \bar{\kappa}\bar{D}^2 - 2\bar{\kappa}\bar{C} + (7/3)\bar{D}\bar{C}]}{\bar{\kappa} - \bar{D} + ((18\varepsilon De_N^2)/\bar{\kappa}^2)(\bar{\kappa}^3 - 6\bar{D} - 3\bar{\kappa}^2\bar{D} + 6\bar{\kappa})}\\ a_3 &= -\frac{9}{2}\frac{\bar{\kappa}^4\varepsilon De_N^2(\bar{D} + (3/2)\bar{\kappa}\bar{C}^2 - (5/2)\bar{D}\bar{C})}{\bar{\kappa} - \bar{D} + ((18\varepsilon De_N^2)/\bar{\kappa}^2)(\bar{\kappa}^3 - 6\bar{D} - 3\bar{\kappa}^2\bar{D} + 6\bar{\kappa})}\end{aligned} \tag{47}$$

The solution of Eq. (46) for Γ_{sp} is Eq. (33), but with the coefficients of Eq. (47).

For $(10 \lesssim \bar{\kappa} \lesssim 10^3)$, $\cosh(\bar{\kappa}) \gg 1$ and $\bar{D} = \tanh(\bar{\kappa}) \approx 1$, and the above equations simplify to become

$$\begin{aligned}a_1 &= \frac{-(\bar{\kappa}\Upsilon_1 + 0.5\bar{\kappa}^2 + 9\varepsilon De_N^2[3\bar{\kappa}^2 - 3\bar{\kappa} + (3/2)])}{\bar{\kappa} - 1 + ((18\varepsilon De_N^2)/\bar{\kappa}^2)(\bar{\kappa}^3 - 3\bar{\kappa}^2 + 6\bar{\kappa} - 6)}\\ a_2 &= \frac{18\bar{\kappa}^2\varepsilon De_N^2[\bar{\kappa} - (1/3)]}{\bar{\kappa} - 1 + ((18\varepsilon De_N^2)/\bar{\kappa}^2)(\bar{\kappa}^3 - 3\bar{\kappa}^2 + 6\bar{\kappa} - 6)}\\ a_3 &= -\frac{9}{2}\frac{\bar{\kappa}^4\varepsilon De_N^2}{\bar{\kappa} - 1 + ((18\varepsilon De_N^2)/\bar{\kappa}^2)(\bar{\kappa}^3 - 3\bar{\kappa}^2 + 6\bar{\kappa} - 6)}\end{aligned} \tag{48}$$

As expected, Eqs. (46)–(47) reduce to the Newtonian fluid solution, as found in [42], when $\varepsilon \to 0$:

$$\Gamma_{sp} = \Upsilon_1\left[\frac{1 + (1/2)(\bar{\kappa}^2/\Upsilon_1)((\bar{D}/\bar{\kappa}) - \bar{C})}{1 - \bar{D}/\bar{\kappa}}\right] \tag{49}$$

3.6. Analytical solutions for the FENE-P model

For fully developed channel flow there is similarity between the solutions for the PTT and the FENE-P models as found by Oliveira [11]. Comparing Eqs. (10)–(12) for the PTT model with Eqs. (14) and (15) for the FENE-P model, and since the momentum Eq. (21) is independent of the constitutive equation, there is an exact equivalence of the solution in the sense of a parameter to parameter match, as explained in detail in Cruz et al. [12]. Hence, the solution of Section 3.4 also applies to the flow of FENE-P fluids, provided the following substitutions are made:

$$\begin{aligned}f(\tau_{xx}) &\to \left(\frac{b+2}{b+5}\right)Z(\tau_{xx})\\ \lambda &\to \lambda\left(\frac{b+2}{b+5}\right)\\ \varepsilon &\to \frac{1}{b+5}\\ \eta &\to \eta\end{aligned} \tag{50}$$

Identically, these same substitutions are valid to provide the pipe solution for the FENE-P model from the corresponding PTT equations in Appendix A.

4. Discussion of results

In the previous section, general equations were derived for fully developed flow of viscoelastic fluids (PTT and FENE-P fluids) under the mixed influence of electrokinetic and pressure gradient forces. The different influences of the driving forces and fluid rheology on the velocity profile have been identified in Eq. (25) and in this

section we discuss in detail some limiting cases in order to understand the fluid dynamics. The following limit cases contained in the general solution are: (a) Newtonian fluid with mixed electro-osmotic/pressure driving forces; (b) viscoelastic fluid under the sole influence of an electro-osmotic driving force; (c) Poiseuille flow of a viscoelastic fluid and (d) viscoelastic fluid with mixed electro-osmotic/pressure driving forces. Case (c) was studied in detail elsewhere [5,7,12], and so was case (a) [26], but this latter situation is revisited here as a starting point.

4.1. Newtonian fluid with mixed driving forces

For a Newtonian fluid the relaxation time is zero and the Deborah number vanishes ($De_\kappa = 0$), thus Eq. (29) becomes

$$\frac{u}{u_{sh}} = 1 - \frac{\cosh(\bar{\kappa}\bar{y})}{\cosh(\bar{\kappa})} - \frac{1}{2}\Gamma(1-\bar{y}^2) \tag{51}$$

under the mixed influence of electro-osmotic and pressure driving forces, as was also shown by Dutta and Beskok [26]. For $\Gamma \to \infty$, pressure forces dominate the momentum transport for any value of $\bar{\kappa}$, and the classical laminar parabolic velocity profile is recovered. Note that this corresponds to $E_x \to 0$ and $u_{sh} \to 0$, since $u_{sh} \propto E_x$ and $\Gamma \propto E_x^{-1}$. For $\Gamma \to 0$, the last term on the right-hand side of Eq. (51) vanishes, the flow becomes governed solely by the electro-osmosis and the velocity profile is only a function of the wall distance and the relative microchannel ratio, $\bar{\kappa}$, as shown earlier by Burgreen and Nakache [23]. Fig. 2 shows the effect of the relative microchannel ratio, $\bar{\kappa}$ (or H/ξ, where ξ is the Debye layer thickness) on the dimensionless velocity profiles for pure electro-osmotic flow, $\Gamma = 0$. As $\bar{\kappa} \to 1$ the double layer thickness becomes of the same order of magnitude as the channel half-height and the region of excess charge is distributed over the entire channel. This situation is not fully compatible with this solution for which the Debye–Hückel approximation was invoked, which requires $\bar{\kappa}_{\min} \gtrsim 10$. For $\bar{\kappa} = 100$ the width the Debye layer is about 1% of the channel half-height. Note that for large $\bar{\kappa}$ ($\bar{\kappa} \to \infty$) the size of the EDL or region of excess charge is relatively small, and Eq. (51) reduces to the classical Helmoltz–Smoluchowski equation, $u/u_{sh} = 1$ [22], if simultaneously $\Gamma = 0$.

Fig. 3 shows velocity profiles for various ratios of pressure gradient to electro-osmotic driving forces at $\bar{\kappa} = 20$ and $\bar{\kappa} = 100$. When $\Gamma = 0$ the velocity profiles correspond to a *pluglike flow*. $\Gamma < 0$ and

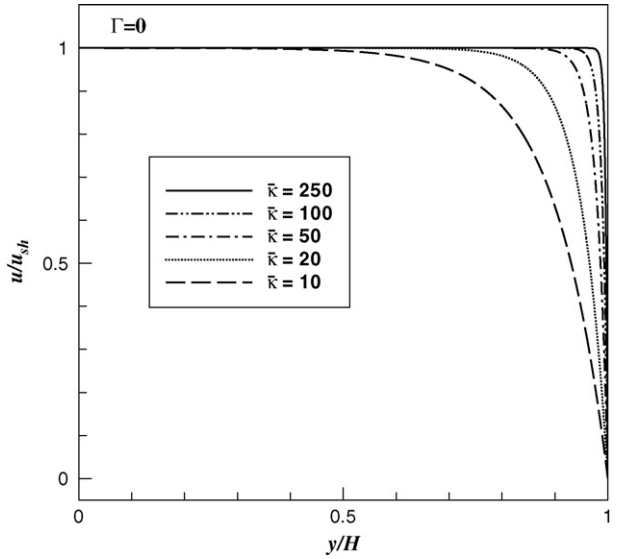

Fig. 2. Velocity profiles for several relative microchannel ratios, $\bar{\kappa}$, for Newtonian fluids under the sole influence of electrokinetic forces, $\Gamma = 0$.

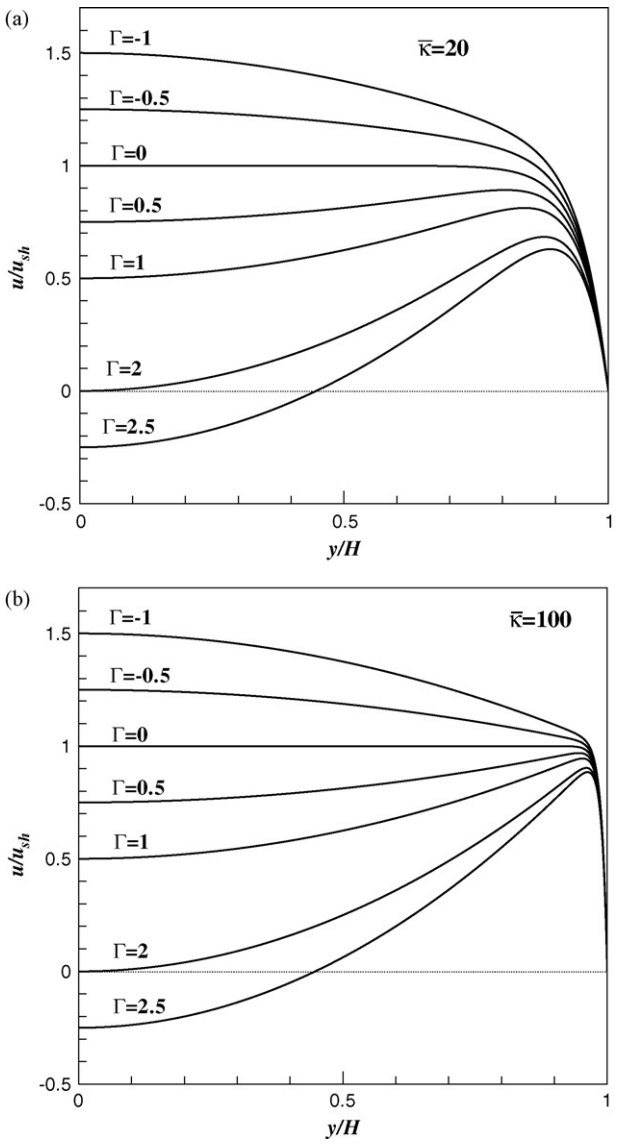

Fig. 3. Velocity profiles for various ratios of pressure to electro-osmotic driving forces, Γ, for Newtonian fluids with relative microchannel ratio of (a) $\bar{\kappa} = 20$ and (b) $\bar{\kappa} = 100$.

$\Gamma > 0$ correspond to Poiseuille electro-osmotic flows with favorable and adverse pressure gradients, respectively. The velocity profiles shown in Fig. 3(b) for $\bar{\kappa} = 100$ are identical to those of Dutta and Beskok [26]. The value of $\bar{\kappa} = 100$ is a typical example for a 0.1 mM buffer solution in a glass channel with ψ_0 of aproximately 25 mV [26].

Eq. (51) predicts negative velocities at $\bar{y} = 0$ when $\Gamma > 2((\cosh(\bar{\kappa}) - 1)/(\cosh(\bar{\kappa})))$ for all values of $\bar{\kappa}$. For small but finite Debye lengths, $\bar{\kappa} \gtrsim 10$, the velocity becomes negative in the central region of the channel for $\Gamma \gtrsim 2$. As shown in Fig. 3, the velocity maxima depend on Γ, and this dependency can be expressed by

$$\begin{cases} \left.\dfrac{u}{u_{sh}}\right|_{\max} = 1 - \dfrac{1}{2}\Gamma & \Gamma \le 0 \bigwedge \bar{\kappa} \gtrsim 10 \\ \left.\dfrac{u}{u_{sh}}\right|_{\max} = 1 - \dfrac{\cosh(\bar{\kappa}\bar{\delta})}{\cosh(\bar{\kappa})} - \dfrac{1}{2}\Gamma(1-\bar{\delta}^2) & \Gamma > 0 \end{cases} \tag{52}$$

where $\bar{\delta}$ is the dimensionless locci of the velocity peaks (or $\tau_{xy\|y=\bar{\delta}} = 0$), given by Eq. (40).

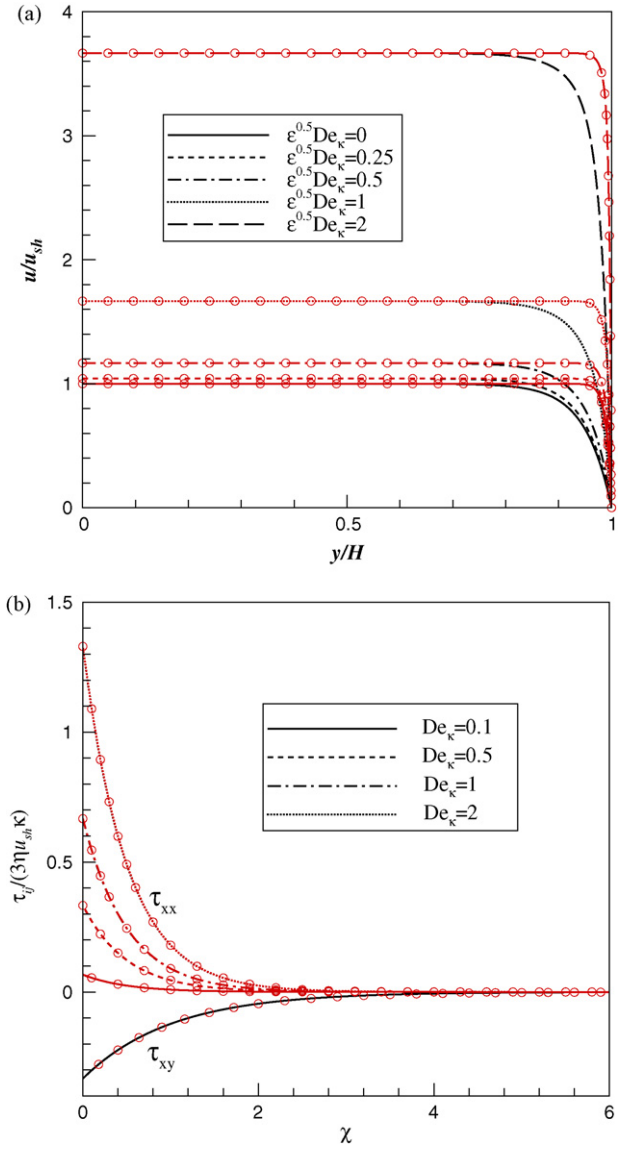

Fig. 4. Flow characteristics for electro-osmotic flow ($\Gamma = 0$) of a PTT fluid for relative microchannel ratios of $\bar{\kappa} = 20$ (lines) and $\bar{\kappa} = 100$ (lines and symbols): (a) dimensionless velocity profiles as function of $\sqrt{\varepsilon}De_\kappa$; (b) dimensionless normal and shear stress profiles as function of De_κ. $\chi = (1 - \bar{y})\bar{\kappa}$ is the near wall variable.

4.2. Viscoelastic fluid with sole electro-osmotic driving force

The discussion in this paper on viscoelastic flows is for a PTT fluid, but will be identical for a FENE-P model provided the substitutions indicated in Section 3.6 are made. For a viscoelastic fluid under the sole influence of electro-osmotic driving force, $\Gamma = 0$, Eq. (29) reduces to

$$\frac{u}{u_{sh}} = \left(1 - 2\frac{\varepsilon De_\kappa^2}{\cosh^2(\bar{\kappa})}\right)\left(1 - \frac{\cosh(\bar{\kappa}\bar{y})}{\cosh(\bar{\kappa})}\right) + \frac{2}{3}\varepsilon De_\kappa^2 \times \left[1 - \left(\frac{\cosh(\bar{\kappa}\bar{y})}{\cosh(\bar{\kappa})}\right)^3\right] \quad (53)$$

Fig. 4(a) shows the corresponding dimensionless velocity profiles as a function of the parameter $\sqrt{\varepsilon}De_\kappa$ for two relative microchannel ratios of $\bar{\kappa} = 20$ and $\bar{\kappa} = 100$ and these profiles should be compared with the profiles in Fig. 2 for Newtonian fluids. As for Newtonian fluids, the velocity profiles exhibit a *pluglike* shape, but now with the velocity plateau increasing significantly with $\sqrt{\varepsilon}De_\kappa$, for both values

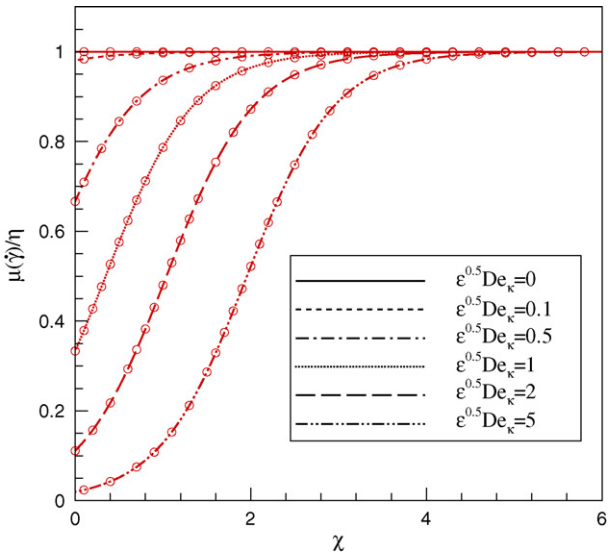

Fig. 5. Dimensionless viscosity profiles for electro-osmotic viscoelastic flow ($\Gamma = 0$) of a PTT fluid as function of $\sqrt{\varepsilon}De_\kappa$ for relative microchannel ratios of $\bar{\kappa} = 20$ (lines) and $\bar{\kappa} = 100$ (lines and symbols). $\chi = (1 - \bar{y})\bar{\kappa}$ is the near wall variable.

of $\bar{\kappa}$. In fact, setting $\bar{y} = 0$ in Eq. (53) leads to the following quadratic relationship between the maximum velocity plateau and $\sqrt{\varepsilon}De_\kappa$,

$$\left.\frac{u}{u_{sh}}\right|_{\max} = \left(1 - 2\frac{\varepsilon De_\kappa^2}{\cosh^2(\bar{\kappa})}\right)\left(1 - \frac{1}{\cosh(\bar{\kappa})}\right) + \frac{2}{3}\varepsilon De_\kappa^2\left[1 - \frac{1}{\cosh^3(\bar{\kappa})}\right] \quad (54)$$

which for $\bar{\kappa} \gtrsim 10$ reduces to $(u/u_{sh})|_{\max} \approx 1 + (2/3)\varepsilon De_\kappa^2$.

The influence of $\bar{\kappa}$ on the velocity profiles of Fig. 4(a) is restricted to a narrow region, the effective EDL thickness, with the velocity profiles for higher values of $\bar{\kappa}$ exhibiting thinner EDL layers and consequently larger velocity gradients. Fig. 4(b) shows the corresponding profiles of dimensionless normal and shear stresses for the viscoelastic fluid as function of De_κ. In order to simplify the analysis of the influence of both De_κ and $\bar{\kappa}$ on the stress profiles, a near-wall variable, $\chi = (1 - \bar{y})\bar{\kappa}$, is used. By using χ in Fig. 4(b) the stress profiles for different values of $\bar{\kappa}$collapse, since their magnitudes are determined by the values of $\bar{\kappa}$. The dimensionless shear stress is also independent of De_κ, exhibiting a constant wall value of $-1/3$ (as predicted by Eq. (35) with $\Gamma = 0$). The normal stresses increase linearly with De_κ regardless of $\bar{\kappa}$ (cf. Eq. (36)).

Dimensionless shear viscosity profiles for the PTT fluid in electro-osmotic flow are plotted in Fig. 5 as function of the near wall variable, χ. There is a decrease in shear viscosity near the wall when $\sqrt{\varepsilon}De_\kappa$ increases, on account of the shear-thinning behavior of the PTT fluid, and consequently the thickness of the EDL is larger than for the equivalent Newtonian flow. By using the modified wall variable the dimensionless shear viscosity profiles, $\bar{\mu}(\dot{\gamma})$, become independent of the relative micro-channel ratio. It is this low wall viscosity at high values of εDe_κ^2 that is responsible for the strong increase in u/u_{sh}.

4.3. Viscoelastic fluid with mixed driving forces

The viscoelastic flow characteristics under the combined action of electro-osmosis and pressure gradient forcing are discussed here, recalling Eq. (25).

Fig. 6(a) and (b) presents dimensionless velocity profiles for flows with favorable and adverse pressure gradients, respectively. For $\Gamma < 0$, the velocity profiles increase with $\sqrt{\varepsilon}De_\kappa$, as seen

previously in Fig. 4, due to shear-thinning effects, leading to correspondingly higher shear rates near the walls. For $\Gamma > 0$, the pressure gradient is against the flow and the velocity profiles show the same double peak seen for Newtonian flows (cf. Fig. 3). The velocity profiles also increase with $\sqrt{\varepsilon}De_\kappa$, due to increasing levels of shear-thinning, both within the EDL layer and in the bulk zone. For flow with favorable pressure gradients the velocity maximum is given by Eq. (55)(for $\bar{\kappa} \gtrsim 10$) and takes place on the centreplane. For adverse pressure gradients the velocity peaks are at the edge of the EDL and the corresponding velocity maximum depends on Γ as given by Eq. (56)

$$\left.\frac{u}{u_{sh}}\right|_{\max} = 1 - \frac{1}{2}\Gamma + \frac{3}{2}\frac{\varepsilon De_\kappa^2}{\bar{\kappa}^2}\Gamma\left[1 - 2\bar{\kappa} + \frac{4}{9}\frac{\bar{\kappa}^2}{\Gamma} + \frac{8}{\bar{\kappa}^2}\Gamma \times \left[1 + \bar{\kappa}\left(\frac{1}{2}\bar{\kappa} - 1\right)\right] - \frac{\Gamma^2}{3}\right], \quad \Gamma \le 0, \bar{\kappa} \gtrsim 10 \tag{55}$$

$$\left.\frac{u}{u_{sh}}\right|_{\max} = \frac{u(\bar{\delta})}{u_{sh}}, \quad \Gamma > 0, \bar{\kappa} \gtrsim 10 \tag{56}$$

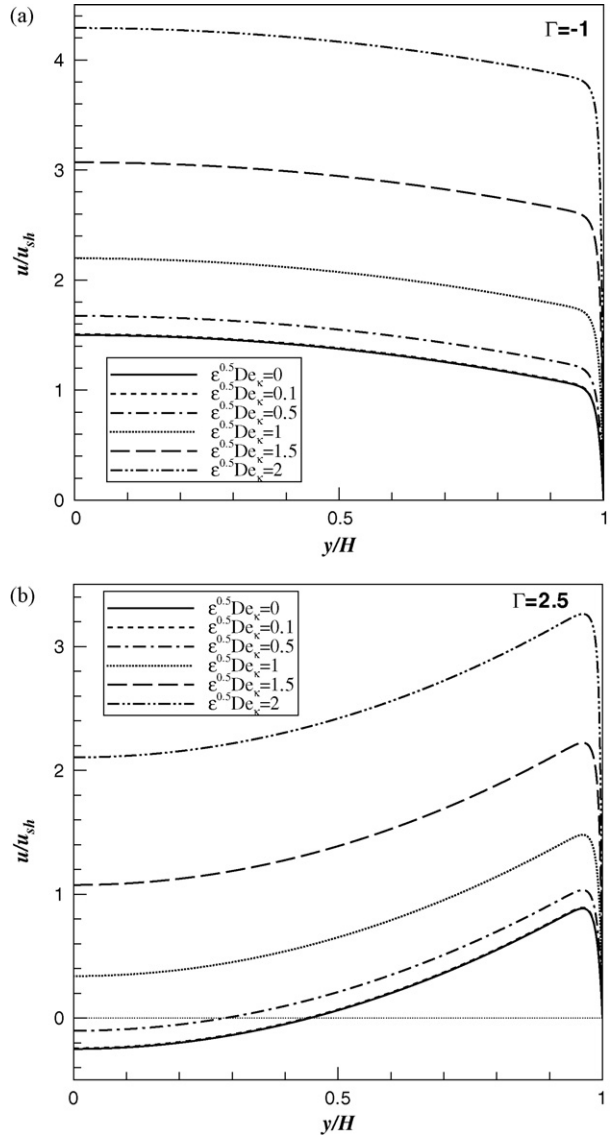

Fig. 6. Dimensionless velocity profiles for a PTT fluid under the mixed influence of electro-osmotic/pressure driving force as function of $\sqrt{\varepsilon}De_\kappa$ relative microchannel ratio of $\bar{\kappa} = 100$: (a) $\Gamma = -1$ and (b) $\Gamma = 2.5$.

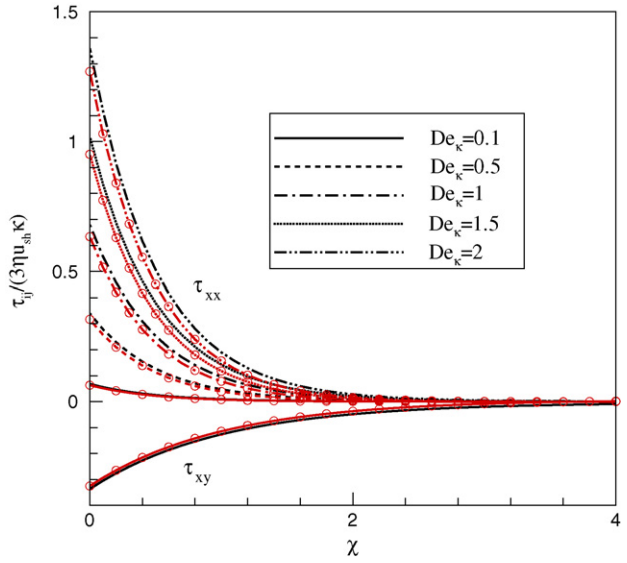

Fig. 7. Profiles of dimensionless normal and shear stresses for viscoelastic fluid under the mixed influence of electro-osmotic/pressure driving force as function of $\sqrt{\varepsilon}De_\kappa$ for $\bar{\kappa} = 100$, $\Gamma = -1$ (lines) and $\Gamma = 2.5$ (lines with symbols).

where $\bar{\delta}$ is the dimensionless locci of the velocity peaks (or the location of a zero shear stress, $\tau_{xy\|y=\bar{\delta}} = 0$) to be calculated from Eq. (40).

Fig. 7 shows transverse profiles of the dimensionless normal and shear stresses as function of the near-wall variable, $\chi = (1 - \bar{y})\bar{\kappa}$ and Deborah number, for a high value of $\bar{\kappa}$ ($\bar{\kappa} = 100$). The lines represent flows with favorable pressure gradients ($\Gamma = -1$) whereas lines with symbols typify flows with adverse pressure gradients ($\Gamma = 2.5$). In the former case the dimensionless normal stresses decrease sharply near the microchannel walls, within the EDL layer, as shown in detail in Fig. 8 for $De_\kappa = 2$. In the latter case, as shown in Fig. 8, the profiles of $\bar{\tau}_{xx}$ also decrease sharply near the microchannel walls within the EDL, followed by an increase to a local maximum at the end of the EDL layer. For all flows the magnitude of $\bar{\tau}_{xx}$ increases with De_κ and $\bar{\kappa}$.

As observed in Section 3.4 in respect to Eq. (25), besides the viscoelastic flow induced by the single contributions from electrical and pressure potentials, there is an extra term that simultaneously

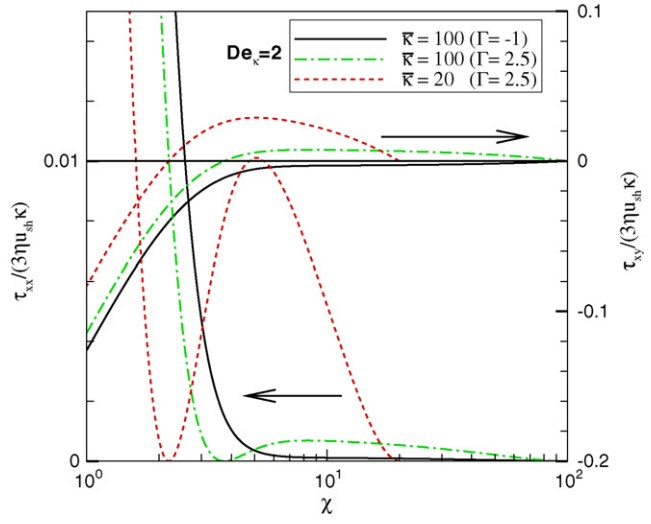

Fig. 8. Profiles of dimensionless normal and shear stresses for viscoelastic fluid under the mixed influence of electro-osmotic/pressure driving force at $De_\kappa = 2$ as function of the near wall variable, for $\bar{\kappa} = 100$ ($\Gamma = -1$ and $\Gamma = 2.5$) and $\bar{\kappa} = 20$ ($\Gamma = 2.5$).

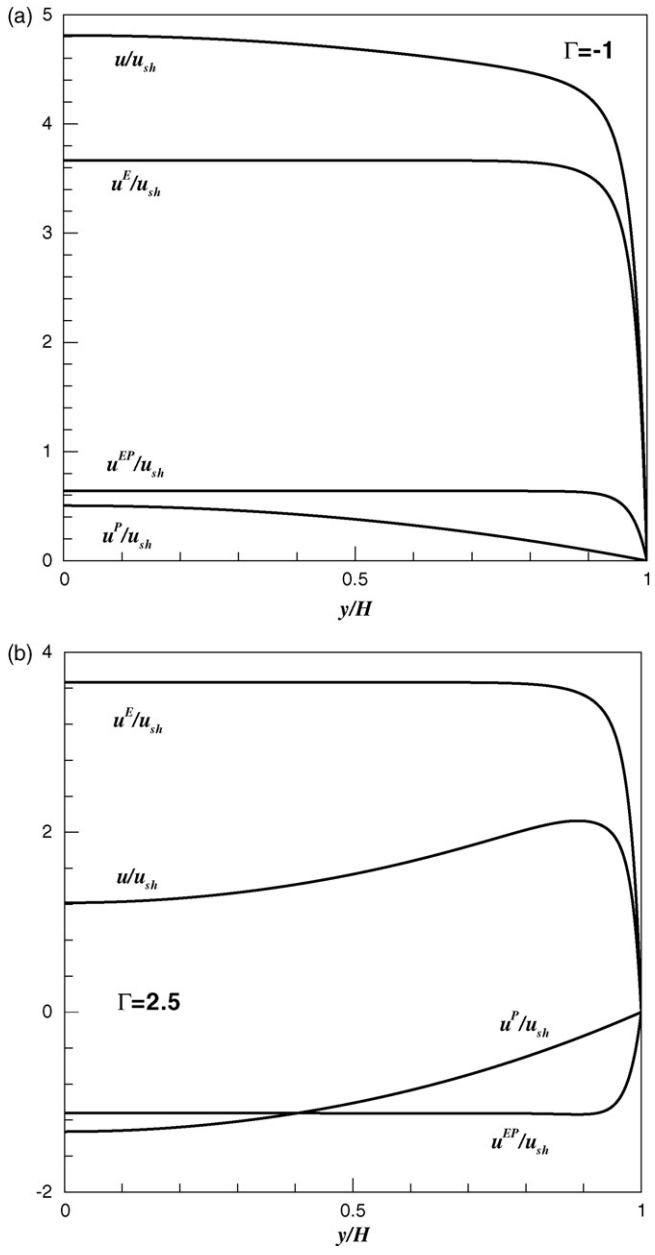

Fig. 9. Profiles of the components of the dimensionless velocity for a PTT fluid under the mixed influence of electro-osmotic/pressure driving force for $\sqrt{\varepsilon}De_\kappa = 2$ and relative microchannel ratio of $\bar{\kappa} = 20$: (a) $\Gamma = -1$ and (b) $\Gamma = 2.5$.

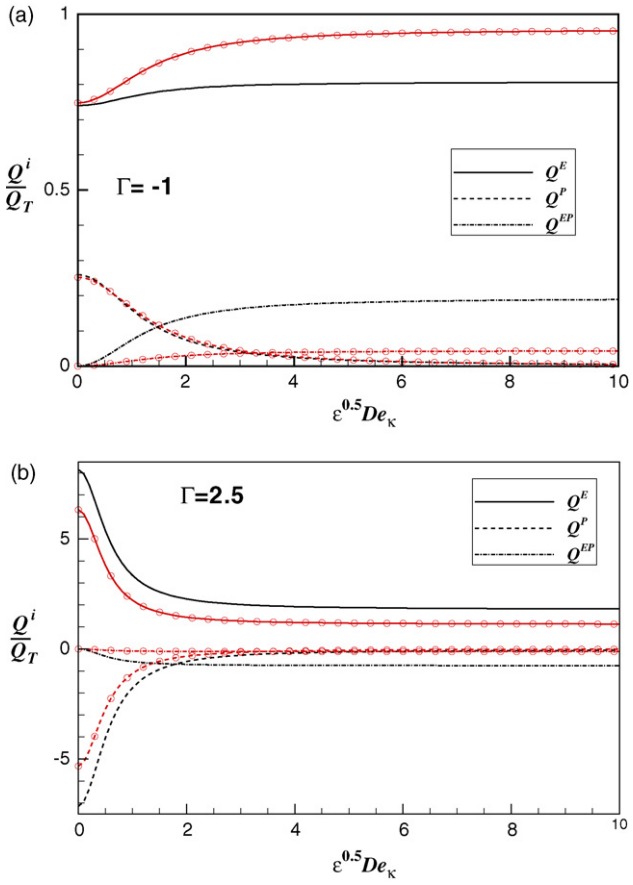

Fig. 10. Relative contributions to the flow rate for electro-osmotic flow of a PTT fluid for relative microchannel ratios of $\bar{\kappa} = 20$ (lines) and $\bar{\kappa} = 100$ (lines and symbols) as function of $\sqrt{\varepsilon}De_\kappa$: (a) $\Gamma = -1$ (b) $\Gamma = 2.5$.

combines both effects and which is absent from the Newtonian case. This invalidates the superposition principle, and is associated with the non-linearity of the rheological model. These various contributions and the corresponding whole velocity profile are plotted in Fig. 9(a) and (b) for two typical cases of favorable and opposed pressure gradient and electric force, $\Gamma = -1$ and $\Gamma = 2.5$, respectively. The combined term u^{EP} acts in the same direction as the Poiseuille contributions, but has a slope like that of the electro-osmotic contribution, i.e., it is a plug like profile except in the wall vicinity. In absolute terms u^{EP} and u^P are here of similar magnitude, but u^{EP} can be larger than u^P as discussed next.

The corresponding flow rates are given by Eq. (30) and the flow rate contributions relative to the total flow rate, $Q_T = Q^E + Q^P + Q^{EP}$, are shown in Fig. 10(a) and (b), as function of $\sqrt{\varepsilon}De_N$ for $\Gamma = -1$ and $\Gamma = 2.5$, respectively. The contribution in terms of flow rate are similar to those of the velocity discussed above, but no longer include the effect of position in the channel. In each figure, curves for two relative microchannel ratios of $\bar{\kappa} = 20$ (lines) and $\bar{\kappa} = 100$ (lines and symbols) are presented. At low $\sqrt{\varepsilon}De_N$ the relative contributions vary quickly from their corresponding Newtonian values to asymptotic values at large $\sqrt{\varepsilon}De_N$ ($\sqrt{\varepsilon}De_N \gtrsim 5$). These asymptotic values at large $\sqrt{\varepsilon}De_N$ are inversely proportional to $\bar{\kappa}$. For $\Gamma = -1$ and $\bar{\kappa} = 20$ the non-linear contribution is actually quite significant, with $Q^{EP}/Q_T \simeq 19\%$, whereas at $\bar{\kappa} = 100$, Q^{EP}/Q_T is only of 4%. At high values of $\sqrt{\varepsilon}De_N$, the non-linear contribution becomes stronger than the pressure potential contribution, because $\bar{Q}^{EP}$ has one term linearly proportional to the pressure gradient and a second term proportional to $p_{,x}^2$, which acts in opposite direction to the linear term for $p_{,x} > 0$. This non-linear contribution is therefore equivalent to a drag reduction effect when fixing the flow rate and quantifying the required forcings relative to a non-coupled situation. For adverse pressure gradients, the non-linear contribution acts to reduce the total flow rate as shown in Fig. 10(b) for $\Gamma = 2.5$, where the non-linear flow reduction, $\bar{Q}^{EP}$, is stronger than the pressure contribution, $\bar{Q}^P$. Thus, the coupled term is now acting as a drag increaser. In this situation, the main contribution for the total flow rate is $\bar{Q}^E$, with both $\bar{Q}^P$ and $\bar{Q}^{EP}$ acting to reduce the flow rate. At higher values of $\sqrt{\varepsilon}De_N$ this reduction is again stronger at lower values of $\bar{\kappa}$, with $Q^{EP}/Q_T \simeq -12\%$ and -76% for $\bar{\kappa} = 100$ and $\bar{\kappa} = 20$, respectively (note that $Q^E/Q_T \simeq 180\%$ for $\bar{\kappa} = 20$).

The variation with Γ of the asymptotic values at $\varepsilon De_\kappa^2 = 200$ of the various contributions to the total flow rate are plotted in Fig. 11 for $\bar{\kappa} = 20$. For very large favorable and adverse pressure gradient the main flow is obviously dominated by the pressure contribution, $\bar{Q}^P$. The singularities at $\Gamma \simeq 6.45$ correspond to $\bar{Q} \simeq 0$. Here,

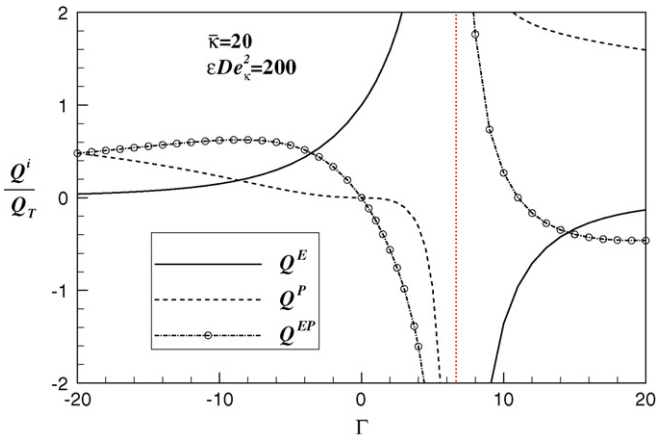

Fig. 11. Relative contributions to the flow rate for electro-osmotic flow of a PTT fluid for relative microchannel ratios of $\bar{\kappa} = 20$ at large $\varepsilon De_{\kappa}^2 (= 200)$ as a function of Γ.

the strength of the adverse pressure gradient was sufficient to overcome the strength of the electro-osmotic forcing to reverse the total flow rate.

To discuss the streaming potential problem it is more enlightning to work with the reciprocal of Γ_{sp}, $\Gamma_{sp}^{-1} = -((\epsilon\psi_0)/H^2)(E_{x,sp}/p_{,x})$. Fig. 12(a) shows that this quantity increases with viscoelasticity, for differents values of $\bar{\kappa}$ and Υ_1. This means that viscoelasticity increases the amount of electrical streaming current,

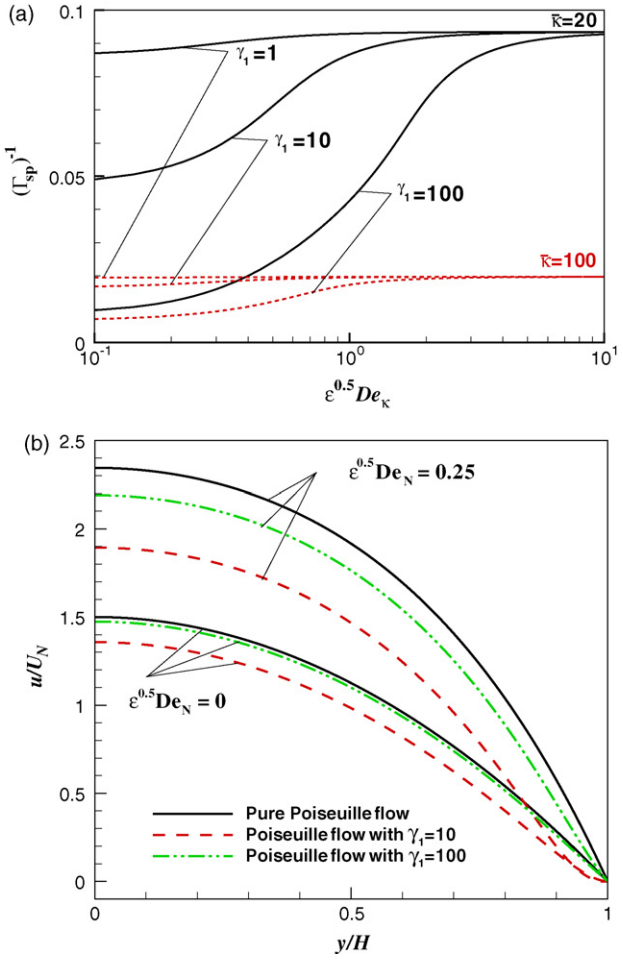

Fig. 12. Streaming potential: (a) variation of Γ_{sp}^{-1} with $\sqrt{\varepsilon}De_N$ as function of $\bar{\kappa}$ and Υ_1; (b) normalized velocity profiles for $\bar{\kappa} = 20$ and showing effects of Υ_1 and $\sqrt{\varepsilon}De_N$.

which asymptotes to a constant value at high $\sqrt{\varepsilon}De_N$. In contrast, increasing Υ_1 decreases the value of Γ_{sp}^{-1} (and the amount of electrical streaming current) for two reasons. The streaming current is directly proportional to $E_{x,sp}$ (cf. Eq. (43)) and then with $I_c' = -I_s'$, a higher electrical conductivity implies a lower value of $E_{x,sp}$ as in Eq. (44). So, the combination of these two effects, for a given pressure gradient results in a lower streaming potential therefore a lower value of Γ_{sp}^{-1}. Similarly, if the system has a lower electrical conductivity stronger streaming potentials are required to obtain electrical equilibrium. The necessarily larger electric fields in poor conductors (small Υ_1) lead to stronger effects on the velocity field as is well shown in Fig. 12(b). Here, the deviation from pure Poiseuille flow is enhanced by poor electric conductivity. This Figure also confirms that viscoelastic shear-thinning fluids enhance streaming potential effects more than Newtonian fluids. All these effects are enhanced as $\bar{\kappa}$decreases. Note that the velocity profiles in Fig. 12(b) have been normalized by the Newtonian bulk velocity at identical pressure gradient (U_N), instead of u_{sh}, to avoid the singularity in the Helmholtz–Smoluchowski electro-osmotic velocity ($E_{x,sp} = 0$) for pure Poiseuille flow.

The final comment concerns with the skimming layer, the thin layer close to the wall where the fluid essentially behaves as the Newtonian solvent. This can act as a lubrication layer and the real impact on the flow depends on the ratio between its thickness (δ_l) and the EDL thickness (ξ), on the amount of shear-thinning of the bulk fluid, on the applied pressure gradient and on the ratio between the characteristic viscosities of the bulk fluid and solvent. For both $\delta_l = \xi$ and $\delta_l > \xi$, u/u_{sh} is essentially unchanged in the EDL for the homogeneous and two-fluid model. Outside the EDL, u/u_{sh} does not change much if the flow is purely electro-osmotic regardless of all other parameters, but an intense shear-thinning can lead to differences of up to 20% as can be assessed from Berli and Olivares [32]. In the presence of a skimming layer the sensitivity of u/u_{sh} to pressure gradient is always reduced relative to the homogeneous fluid solution: for $\delta_l = \xi$ this leads to large differences in u/u_{sh} outside the EDL and for $\delta_l > \xi$, say $\delta_l = 5\xi$, this problem is somewhat reduced so that for weak shear-thinning fluids (and Newtonian fluids) the homogeneous solution is a good approximation to the two-fluid model, but for moderate to strongly shear-thinning fluids differences in excess of 70% can be found. This is currently a problem under investigation for viscoelastic fluids.

5. Conclusions

Analytical solutions for channel and pipe flows of viscoelastic fluids under the mixed influence of electrokinetic and pressure forces were obtained. The analysis are restricted to cases with small electric double-layer, where the distance between the walls of a microfluidic device is at least one order of magnitude larger than the EDL. The viscoelastic fluids used are described by the PTT model (Phan-Thien and Tanner [3]), with linear kernel for the stress coefficient function and zero second normal stress difference [4], and the FENE-P model [10].

In the absence of an imposed pressure gradient, the electro-osmotic flow exhibits a pluglike velocity profile, as found previously for Newtonian fluids, but with the maximum velocity plateau increasing quadraticaly with $\sqrt{\varepsilon}De_{\kappa}$, for all $\bar{\kappa}$ values.

When the viscoelastic flow is induced by a combination of both electrical and pressure potentials, in addition to the single contributions from these two mechanisms, there is an extra term in the velocity profile that simultaneously combines both, which is absent for the Newtonian case where the superposition principle applies. This non-linear term can contribute significantly to the total flow rate, depending on the value of $\bar{\kappa}$. Under conditions of favorable pressure gradient it thus acts as a drag reducer, but for adverse

pressure gradients it changes its role to become a drag increaser. Its existence invalidates the superposition principle and is associated with the non-linearity of the rheological model, with this analytical solution indicating that for quasi-linear viscoelastic equations the superposition principle still applies.

Under favorable pressure gradients, the velocities increase significantly with $\sqrt{\varepsilon}De_\kappa$, with the profiles at higher values of $\bar{\kappa}$ exhibiting large shear rates within the electric double layer. As for Newtonian fluids, adverse pressure gradients lead to local velocity peaks at the edge of the electric double layer.

Regarding the streaming potential problem, viscoelasticity increases the amount of electrical streaming current, which asymptotes to a constant value at high $\sqrt{\varepsilon}De_N$. The amount of electrical streaming current decreases with the increase of Υ_1, due to the lower $E_{x,sp}$ required to establish the conduction current for good conductors and the consequent lower streaming potential as found for Newtonian fluids.

Acknowledgements

The authors acknowledge funding from FEDER and Fundação para a Ciência e a Tecnologia (FCT), Portugal, through projects PPCDT/EME/59338/2004, PTDC/EQU-FTT/70727/2006 and PTDC/EQU-FTT/71800/2006. A. Afonso would also like to thank FCT for financial support through the scholarship SFRH/BD28828/2006. The help of Dr. S. Dhinakaran in checking the equations is gratefully acknowledged.

Appendix A. Analytical solution for the PTT and FENE-P models in pipe flow

The momentum equation is given by Eq. (A.1) where now y denotes the radial coordinate, H is the pipe radius and all other quantities are defined in the main text. The net charge density distribution is given by Eq. (20)

$$\frac{1}{y}\frac{\mathrm{d}(y\tau_{xy})}{\mathrm{d}y} = -\rho_e E_x + p_{,x} \tag{A.1}$$

which can be integrated to obtain

$$\tau_{xy} = \frac{\epsilon\psi_0 E_x \kappa \sinh(\kappa y)}{\cosh(\kappa H)} - \frac{\epsilon\psi_0 E_x \cosh(\kappa y)}{y\cosh(\kappa H)} + \frac{\epsilon\psi_0 E_x}{y\cosh(\kappa H)} + \frac{1}{2}p_{,x}y \tag{A.2}$$

Using Eq. (13) the following explicit expression for the normal stress component is obtained for the PTT fluid,

$$\tau_{xx} = 2\frac{\lambda}{\eta}\left(\frac{\epsilon\psi_0 E_x \kappa \sinh(\kappa y)}{\cosh(\kappa H)} + \frac{1}{2}p_{,x}y - \frac{\epsilon\psi_0 E_x \cosh(\kappa y)}{y\cosh(\kappa H)} + \frac{\epsilon\psi_0 E_x}{y\cosh(\kappa H)}\right)^2 \tag{A.3}$$

The velocity gradient is

$$\begin{aligned}\dot{\gamma} \equiv \frac{\mathrm{d}u}{\mathrm{d}y} = {} & \left[1 + 2\varepsilon\lambda^2\left(\frac{\epsilon\psi_0 E_x \kappa \sinh(\kappa y)}{\eta\cosh(\kappa H)} + \frac{1}{2\eta}p_{,x}y \right.\right. \\ & \left.\left. - \frac{\epsilon\psi_0 E_x \cosh(\kappa y)}{\eta y\cosh(\kappa H)} + \frac{\epsilon\psi_0 E_x}{\eta y\cosh(\kappa H)}\right)^2\right] \\ & \times \left(\frac{\epsilon\psi_0 E_x \kappa \sinh(\kappa y)}{\eta\cosh(\kappa H)} + \frac{1}{2\eta}p_{,x}y \right. \\ & \left. - \frac{\epsilon\psi_0 E_x \cosh(\kappa y)}{\eta y\cosh(\kappa H)} + \frac{\epsilon\psi_0 E_x}{\eta y\cosh(\kappa H)}\right)\end{aligned} \tag{A.4}$$

The integration of Eq. (A.4) subject to the no-slip boundary condition at the wall ($u_{\|y=H} = 0$) gives the following velocity profile for the PTT fluid:

$$u = u^E + u^P + u^{EP} \tag{A.5}$$

with

$$\begin{aligned}u^E = {} & \left[\frac{\epsilon\psi_0 E_x}{\eta}\right]\left[\bar{A} - 1 + \sqrt{\bar{C}}\left\{\ln\left(\frac{y}{H}\right) + \mathrm{Chi}(\kappa H) - \mathrm{Chi}(\kappa y)\right\}\right] \\ & + \kappa^2 2\varepsilon\lambda^2\left[\frac{\epsilon\psi_0 E_x}{\eta}\right]^3\left[\bar{C}(1-\bar{A}) + \frac{1}{3}(\bar{A}^3 - 1)\right. \\ & + \bar{C}\left\{\sqrt{\bar{C}}\left(\frac{21}{8}\mathrm{Chi}(\kappa y) - \frac{21}{8}\mathrm{Chi}(\kappa H)\right.\right. \\ & + \frac{3}{2}\mathrm{Chi}(2\kappa H) - \frac{3}{2}\mathrm{Chi}(2\kappa y) + \frac{3}{8}\mathrm{Chi}(3\kappa y) \\ & \left.\left. - \frac{3}{8}\mathrm{Chi}(3\kappa H) + \frac{3}{2}\ln\left(\frac{H}{y}\right)\right)\right. \\ & + \frac{3}{2\kappa H}\left[\frac{5}{4}\bar{D}\left(1 - \frac{H}{y}\bar{B}\right) + \sqrt{\bar{C}}\left(\frac{H}{y}\sinh(2\kappa y) - \sinh(2\kappa H)\right.\right. \\ & \left.\left. - \frac{1}{4}\frac{H}{y}\sinh(3\kappa y) + \frac{1}{4}\sinh(3\kappa H)\right)\right] \\ & + \frac{3}{4\kappa^2 H^2}\left[\frac{5}{2}\left(\frac{H^2}{y^2}\bar{A} - 1\right) + \sqrt{\bar{C}}\left(\cosh(2\kappa H) - \frac{H^2}{y^2}\cosh(2\kappa y)\right.\right. \\ & \left.\left.\left. + \frac{5}{3}\left(1 - \frac{H^2}{y^2}\right) + \frac{1}{6}\frac{H^2}{y^2}\cosh(3\kappa y) - \frac{1}{6}\cosh(3\kappa H)\right)\right]\right\}\Bigg]\end{aligned} \tag{A.6}$$

$$u^P = \frac{1}{2}\left[\frac{p_{,x}}{2\eta}\right](y^2 - H^2)\left[1 + \left[\frac{p_{,x}}{2\eta}\right]^2\varepsilon\lambda^2(y^2 + H^2)\right] \tag{A.7}$$

$$\begin{aligned}u^{EP} = {} & \frac{3}{2}\varepsilon\lambda^2\left[\frac{\epsilon\psi_0 E_x}{\eta}\right]^2\left[\frac{p'_x}{2\eta}\right][5(1-\bar{A}^2) + 2\kappa\bar{D}(y\bar{A}\bar{B} - H) \\ & + \kappa^2\bar{C}(H^2 - y^2) + 2\{4\sqrt{\bar{C}}(\bar{A} - 1) + \bar{C}[4\mathrm{Chi}(\kappa H) - 4\mathrm{Chi}(\kappa y) \\ & + \mathrm{Chi}(2\kappa y) - \mathrm{Chi}(2\kappa H) + 3\ln(\frac{y}{H})]\} + 12\frac{\varepsilon\lambda^2}{\kappa^2}\left[\frac{\epsilon\psi_0 E_x}{\eta}\right]\left[\frac{p'_x}{2\eta}\right]^2 \\ & \times \left[\frac{3}{2}\kappa\bar{D}(H - y\bar{B}) + \left(1 + \frac{1}{2}\kappa^2 y^2\right)\bar{A} - \left(1 + \frac{1}{2}\kappa^2 H^2\right)\right. \\ & \left. + \frac{1}{2}\left(\bar{A} - 1 + \frac{\kappa^2}{2}\sqrt{\bar{C}}(y^2 - H^2)\right)\right]\end{aligned} \tag{A.8}$$

where $\mathrm{Chi}(z)$ is the hyperbolic cosine integral, defined as

$$\mathrm{Chi}(z) = \gamma + \ln(z) + \int_0^z \frac{\cosh(t) - 1}{t}\mathrm{d}t \tag{A.9}$$

and γ is the Euler–Mascheroni constant ($\gamma = 0.57721566490\ldots$). $\mathrm{Chi}(z)$ can also be calculated from:

$$\mathrm{Chi}(z) = \gamma + \ln(z) + \frac{1}{2}\sum_{k=1}^{\infty}\frac{z^{2k}}{k(2k)!} \tag{A.10}$$

To obtain the solution for pipe flow of FENE-P fluids it suffices to apply the substitutions of Section 3.6 to this set of equations.

For pipe flow, the relation between the electrical streaming current and the electrical conduction current is

$$I_s = -I_c = \int_0^H 2\pi u(y)\rho_e(y)ydy = -\pi\sigma_t E_{x,sp}H^2 \quad \text{(A.11)}$$

For the PTT and FENE-P fluids, Eq. (A.11) is not integrable, and a numerical approach is required to obtain a solution.

References

[1] H. Lamb, Hydrodynamics, 6th edition, Cambridge University Press, Cambridge, UK, 1932.
[2] A.H.P. Skelland, Non-Newtonian Flow and Heat Transfer, John Wiley & Sons, New York, 1967.
[3] N. Phan-Thien, R.I. Tanner, New constitutive equation derived from network theory, J. Non-Newtonian Fluid Mech. 2 (1977) 353–365.
[4] N. Phan-Thien, A non-linear network viscoelastic model, J. Rheol. 22 (1978) 259–283.
[5] P.J. Oliveira, F.T. Pinho, Analytical solution for fully developed channel and pipe flow of Phan-Thien–Tanner fluids, J. Non-Newtonian Fluid Mech. 387 (1999) 271–280.
[6] F.T. Pinho, P.J. Oliveira, Axial annular flow of a nonlinear viscoelastic fluid—an analytical solution, J. Non-Newtonian Fluid Mech. 93 (2000) 325–337.
[7] M.A. Alves, P.J. Pinho, F.T. Oliveira, Study of steady pipe and channel flows of a single-mode Phan Thien–Tanner fluid, J. Non-Newtonian Fluid Mech. 101 (2001) 55–76.
[8] D.O.A. Cruz, F.T. Pinho, Skewed Poiseuille-Couette flows of sPTT fluids in concentric annuli and channels, J. Non-Newtonian Fluid Mech. 121 (2004)1–14.
[9] M. Mirzazadeh, M.P. Escudier, F. Rashidi, S.H. Hashemabadi, Analytical solution of purely tangential flow for PTT viscoelastic fluid through concentric annulus, J. Non-Newtonian Fluid Mech. 129 (2005) 88–97.
[10] R.B. Bird, P.J. Dotson, N.L. Johnson, Polymer solution rheology based on a finitely extensible bead-spring chain model, J. Non-Newtonian Fluid Mech. 7 (1980) 213–235.
[11] P.J. Oliveira, An exact solution for tube and slit flow of a FENE-P fluid, Acta Mech. 158 (2002) 157–167.
[12] D.O.A. Cruz, F.T. Pinho, P.J. Oliveira, Analytical solutions for fully developed laminar flow of some viscoelastic liquids with a Newtonian solvent contribution, J. Non-Newtonian Fluid Mech. 132 (2005) 28–35.
[13] D.O.A. Cruz, F.T. Pinho, Fully-developed pipe and planar flows of multimode viscoelastic fluids, J. Non-Newtonian Fluid Mech. 141 (2007) 85–98.
[14] G. Schleiniger, R.J. Weinacht, Steady Poiseuille flows for a Giesekus fluid, J. Non-Newtonian Fluid Mech. 40 (1991) 79–102.
[15] J.J. Van Schaftingen, M.J. Crochet, Analytical and numerical solution of the Poiseuille flow of a Johnson–Segalman fluid, J. Non-Newtonian Fluid Mech. 18 (1985) 335–351.
[16] M.M. Fyrillas, G.C. Georgiou, D. Vlassopoulos, Time dependent plane Poiseuille flow of a Johnson–Segalman fluid, J. Non-Newtonian Fluid Mech. 82 (1999) 105–123.
[17] H.A. Stone, A.D. Stroock, A. Ajdari, Engineering flows in small devices: microfluidics toward a Lab-on-a-Chip, Annu. Rev. Fluid Mech. 36 (2004) 381–411.
[18] R.M. Jendrejack, E.T. Dimalanta, D.C. Schwartz, M.D. Graham, J.J. de Pablo, DNA dynamics in a microchannel, Phys. Rev. Lett. 91 (2003) 038102.
[19] H. Bruus, Theoretical Microfluidics, Oxford Master Series in Condensed Matter Physics, Oxford University Press, Oxford, UK, 2008.
[20] F.F. Reuss, Sur un nouvel effet de l'électricité galvanique, Mémoires de la Societé Impériale des Naturalistes de Moscou 2 (1809) 327–337.
[21] H. Helmholtz, Über den Einfluß der elektrischen Grenzschichten bei galvanischer Spannung und der durch Wasserströmung erzeugten Potentialdifferenz, Ann. 7 (1879) 337.
[22] M. von Smoluchowski, Versuch einer mathematischen Theorie der Koagulationskinetic kolloid Lösungen, Z. Phys. Chem. 92 (1917) 129–135.
[23] D. Burgreen, F.R. Nakache, Electrokinetic flow in ultrafine capillary slits, J. Phys. Chem. 68 (1964) 1084–1091.
[24] C.L. Rice, R. Whitehead, Electrokinetic flow in a narrow cylindrical capillary, J. Phys. Chem. 69 (1965) 4017–4024.
[25] S. Levine, J.R. Marriott, G. Neale, N. Epstein, Theory of electrokinetic flow in fine cylindrical capillaries at high zeta-potentials, J. Colloid Interface Sci. 52 (1975) 136.
[26] P. Dutta, A. Beskok, Analytical solution of combined electroosmotic/pressure driven flows in two-dimensional straight channels: finite Debye layer effects, Anal. Chem. 73 (2001) 1979–1986.
[27] S. Arulanandam, D. Li, Liquid transport in rectangular microchannels by electroosmotic pumping, Colloids Surf. A. 161 (2000) 29–102.
[28] C. Wang, T.N. Wong, C. Yang, K.T. Ooi, Characterization of electro-osmotic flow in rectangular microchannels, Int. J. Heat Mass Transf. 50 (2007) 3115–3121.
[29] G. Karniadakis, A. Beskok, N. Aluru, Microflows and nanoflows. Fundamentals and Simulation. Interdisciplinary Applied Mathematics Series, vol. 29, Spinger–Verlag, 2005.
[30] S. Das, S. Chakraborty, Analytical solutions for velocity, temperature and concentration distribution in electroosmotic microchannel flows of a non-Newtonian bio-fluid, Anal. Chim. Acta 559 (2006) 15–24.
[31] S. Chakraborty, Electroosmotically driven capillary transport of typical non-Newtonian biofluids in rectangular microchannels, Anal. Chim. Acta 605 (2007) 175–184.
[32] C.L.A. Berli, M.L. Olivares, Electrokinetic flow of non-Newtonian fluids in microchannels, J. Colloid Interface Sci. 320 (2008) 582–589.
[33] S. Chakkraborty, Dynamics of capillary flow of blood into a microfluidic channel, Lab-on-a-chip 5, (2005) 421–430.
[34] H.M. Park, W.M. Lee, Helmholtz–Smoluchowski velocity for viscoelastic electroosmotic flows, J. Colloid Interface Sci. 317 (2008) 631–636.
[35] R.G. Owens, A new microstructure-based constitutive model for human blood, J. Non-Newtonian Fluid Mech. 140 (2006) 57–70.
[36] M. Moyers-Gonzalez, R.G. Owens, J. Fang, A non-homogeneous constitutive model for human blood. Part I: Model derivation and steady flow, J. Non-Newtonian Fluid Mech. 617 (2008) 327–354.
[37] A. Vissink, H.A. Waterman, E.J. Gravermade, A.K. Panders, A. Vermey, Rheological properties of saliva substitutes containing mucin, carboxymethyl cellulose or polyethylenoxide, J. Oral Pathol. Med. 13 (1984) 22–28.
[38] G.B. Thurston, H. Greiling, Viscoelastic properties of pathological synovial fluids for a wide range of oscillatory shear and frequencies, Rheol. Acta 17 (1978) 433–445.
[39] H. Fam, J.T. Bryant, M. Konopoulou, Rheological properties of synovial fluids, Biorheology 44 (2007) 59–74.
[40] L.E. Rodd, J.J. Cooper-White, D.V. Boger, G.H. McKinley, Role of the elasticity number in the entry flow of dilute polymer solutions in microfabricated contraction geometries, J. Non-Newtonian Fluid Mech. 143 (2007) 170–191.
[41] C. Yang, D. Li, Electrokinetic effect on pressure-driven liquid flows in rectangular microchannels, J. Colloid Interface Sci. 194 (1997) 95–107.
[42] G.M. Mala, D. Li, J.D. Dale, Heat transfer and fluid flow in microchannels, Int. J. Heat Mass Transfer 40 (1997) 3079–3088.